Defect Characterization of Erbium Doped Silicon Light Emitting Diodes

by

Rita Gupta

B.S. Physics, The Pennsylvania State University, 1992

Submitted to the Department of Materials Science and Engineering
in partial fulfillment of the requirements for the degree of

Master of Science in Materials Science

at the

MASSACHUSETTS INSTITUTE OF TECHNOLOGY

August 1994

Author .....
Department of Materials Science and Engineering
August 5, 1994

Certified by .....
Lionel C. Kimerling
Thomas Lord Professor of Materials Science and Engineering
Thesis Supervisor

Accepted by .....
Carl V. Thompson II
Professor of Electronic Materials
Chair, Departmental Committee on Graduate Students

Defect Characterization of Erbium Doped Silicon Light Emitting Diodes

by

Rita Gupta

Submitted to the Department of Materials Science and Engineering
on August 5, 1994, in partial fulfillment of the
requirements for the degree of
Master of Science in Materials Science

Abstract

In this thesis, the defects in Si:Er LED's introduced during processing were studied. The LED's EL and CL spectra exhibit peaks characteristic not only to the Er luminescence, at 1.54μm, but also to dislocation luminescence at lower wavelengths. The defects were found to extend from the surface through the end of the implanted region, using SEM characterization techniques of EBIC and CL. Depth profiles of CL signals show the origin of the dislocation signals, as well as the peak of the Er implant at a depth of 1.5μm. Imaging of defects using either CL or EBIC was difficult, due to the density of dislocations, on the order of $10^8 cm^{-2}$, found from dislocation pit counts. The dislocations were found to be caused by a processing step during fabrication, in particular the implantation damage anneal, occurring after the Er implantation step. The problems with the furnace anneal include transition metal contamination, temperature ramps, and rapid thermal quenching. The dislocations in the devices affect device quality and Er luminescence intensity, because they act as recombination sites for charge carriers, and compete with the Er recombination, as seen in the PL, EL, and CL spectra.

The Er implant was found to be a gaussian profile, even after device processing, through both C-V measurements and CL signal analysis. EBIC efficiency measurements show that Er excitation saturates, after which no further excitation in the Er 4f electron shell occurs. This conclusion shows us that the excited Er ions will only emit light at 1.54μm, the energy released from the transition from the $^4I_{13/2} \rightarrow ^4 I_{15/2}$ in the Er 4f electron shell. By maximizing the concentration of optically active Er ions in the Si lattice, the saturation level of the Er can be increased, resulting in a stronger Er luminescence signal. The ultimate goal of this project is to fabricate devices that will exhibit strong luminescence at room temperature, making Si:Er a viable alternative for future optoelectronic technology.

Thesis Supervisor: Lionel C. Kimerling
Title: Thomas Lord Professor of Materials Science and Engineering

Acknowledgments

I would like to thank my advisor, Professor L.C. Kimerling, for his advice and guidance through the course of my research here. He has taught me much about life as well as research, and I couldn't have picked a better advisor. I would like to thank Drs. Jurgen Michel and Jorg Palm, without whom this reasearch would never have been completed. It has been a pleasure working with them and I am especially grateful for their helpful discussions and all the things they have taught me over the past two years. I am deeply indebted to Bo Zheng, for providing me with as many samples as I wanted, and I would like to acknowledge Sang Ahn, Sang Zhao, and Hichem M'saad, for their help in sample preparation and their equipment expertise .

It would be impossible to thank everyone that has helped me out in some way, so I would like to thank the entire Kimerling group, for making feel like part of the family, and all the support staff, for making things easier. Special thanks to Kate Paterson for listening to me when I needed an ear, and to Mike Morse, who picked me up off the ground when I most needed it. Finally, I would like to thank my father, for his support in everything that I do.

Contents

List of Figures

List of Tables

Chapter 1

Introduction

1.1 Optoelectronic Technology

In an ever increasing need for faster, smaller devices, optoelectronic technology will become the next step in the future of microelectronic chips. Telecommunications will operate with light signals, as optical fibers and waveguides join together on a single chip [1]. Researchers visualize photonic links connecting equipment, such as printed circuit boards, multi-chip modules, and equipment frames, along with services, such as television, and telephone, as early as the year 2010 [1]. In today's electronics, limitations are due to the increase in device packing density, which results in many more metal interconnects and vias. Interconnections in state of the art devices are now as small as 2μm, but as the wires get thinner and closer together, the problems get more complicated, such as cross talk, clock skew and transmission bandwidth [2]. The high speed of todays smaller circuits cannot be completely utilized if the interconnections are the limiting steps. Optical interconnection which alleviates the problems associated with metal wires and high density packaging is simply the next step in electronic technology.

Although much of the research in optoelectronics is focusing on the III-V compounds such as GaAs, a silicon based technology would be desireable. The LED's and lasers that are used today in optoelectronics are primarily made from epitaxial film growth of III-V compounds such as GaAs and InP, utilizing time consuming

growth methods, which result in expensive devices. The integration of III-V compounds with silicon is an idea still being researched, but one that has proven to be difficult, especially with the large lattice mismatch between some III-V's, like GaAs, and Si. Currently growth of GaAs on Si has yielded layers with dislocations greater than $10^6 cm^{-2}$, which is unsuitable for device performance.

Silicon is the most used material today in the microelectronic industry, with more than ten million devices integrated on one chip. Since silicon technology is the most advanced of the semiconductor technologies, integration of silicon and optoelectronic materials would seem to be the most efficient method of achieving the goal of optoelectronic devices. An effective system must have emitters, detectors and processors of optical signals, as well as compatibility with high density packaging [3]. If the technology used is easily integrated into the existing standards for microelectronics, silicon optoelectronic devices may be a breakthrough in modern electronics, revolutionizing the way we communicate.

1.2 Erbium Doped Silicon

To use the properties of existing optical fibers and waveguides, an optoelectronic device must utilize the correct wavelength of light. In SiO_2, light loss is minimized at the wavelength of 1.55 μm, in the infrared range [4]. If SiO_2 is to be used in the optoelectronic devices as a waveguide, a light source in silicon must be found to take advantage of the low losses at particular wavelengths of light. Light output in materials with an indirect gap, like Si, is difficult, due to the phonon interactions during recombination events. The first papers published on light emission of Er doped Si were in 1983 , yielding light at 1.54μm in silicon, despite the indirect bandgap of the material [5].

Erbium doped silicon luminesces due to the intra shell $4f$ transition of the optically active Er^{3+} ion. Light is generated by the internal de-exitation of the core states $^4I_{13/2} \rightarrow {}^4I_{15/2}$ [6]. Because of this intra-shell transition, Er luminesces in all host material in which there is a crystal field interaction [7]. The 4f electrons in the

Er^{3+} ions in the Si lattice are strongly localized, and do not participate in lattice bonding,making the luminescence of the Er independent of the operating temperature of the devices [6]. It has been shown that O, F, C, and N ligands are effective in promoting optical activity of Er, and these elements are employed in fabricating devices, which will be discussed later [8].

As Si:Er is being researched, its potential is increasing as the first integratable optoelectronic technology. The wavelength that is emitted is compatible with existing optical fibers, and is also at the absorption minimum of silica, which makes Si:Er a perfect candidate for optoelectronics [9]. Erbium doped silicon devices will be easily integrated into IC's in which the waveguides can be silicon itself, and be processed on the chip itself to overcome high interconnection densities and bandwidth limitations. The problems in achieving room temperature luminescence are the motivation in pursuing this research. Although the diodes luminesce very strongly at liquid helium temperatures, their light output decreases significantly at normal operating temperatures. In order for this novel technology to be useful, the light output at room temperature must be maximized.

1.2.1 Si:Er Light Emitting Diode

In this thesis, erbium doped silicon light emitting diodes are characterized for their luminescence properties and the defects that arise during processing. The LED's are fabricated on p-type Cz (100) wafers, boron doped to between $0.5 - 2\Omega cm$. There are three slightly different sets of diodes, whose primary processing steps are outlined below.

Diode set G7

- $430\mathring{A}$ thermal oxide
- Er and O implant at 1.5μm. Concentration of Er= $5x10^{17}cm^{-3}$ and O= $3x10^{18}cm^{-3}$, at 4.5 MeV
- Pattern transfer of mesa

- RIE etch of mesa
- p+ implant, for contact. Boron at 40 keV, dose= $7x10^{15}cm^{-2}$
- Junction implant on top of mesa. Phosphorus at 80 keV, dose= $7x10^{15}cm^{-2}$
- Er and junction anneal. 900°C, 20 minutes, oxygen ambient
- Contact deposition and patterning
- Sinter, final oxide thickness =300$\mathring{A}$

Diode set B-4

- 220$\mathring{A}$ thermal oxide
- Junction implant. Arsenic at 90 keV, dose= $7x10^{15}cm^{-2}$
- p+ implant for backside contact. Boron at 40 keV, dose= $7x10^{15}cm^{-2}$
- Junction anneal. 900°C, 30 minutes, nitrogen ambient
- Er and O implant at 1.5μm. Concentration of Er= $5x10^{17}cm^{-3}$ and O= $3x10^{18}cm^{-3}$, at 4.5 MeV
- Mesa pattern and RIE etch
- Er anneal. 900°C, 30 minutes, nitrogen ambient
- Oxide depostion, 3000$\mathring{A}$
- Contact deposition and patterning
- Sinter, final oxide thickness = 2000$\mathring{A}$

Diode set C-2

- Mesa pattern and RIE etch
- 220$\mathring{A}$ thermal oxide

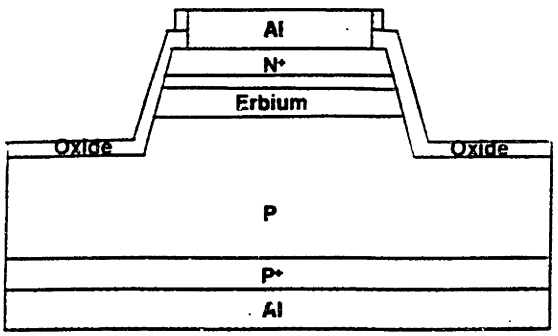

Figure 1-1: Typical cross section of an Si:Er LED

- p+ pattern and implant. Boron at 40 keV, dose= $7x10^{15}cm^{-2}$
- Junction pattern and implant. Phosphorus at 80 keV, dose= $7x10^{15}cm^{-2}$
- Junction anneal. 900°C, 30 minutes, nitrogen ambient
- Er pattern (3 μm photoresist)
- Er and O implant. Concentration of Er= $5x10^{17}cm^{-3}$ and O= $3x10^{18}cm^{-3}$, at 4.5 MeV
- LTO deposition 4000$\mathring{A}$
- Er anneal. 900°C, 30 minutes, Nitrogen ambient
- Contact depositon and patterning
- Sinter, final oxide thickness = 3400$\mathring{A}$

A typical device cross section is shown in Figure 1-1

Electroluminescence spectra were taken of these devices and it was found that there are defect associated luminescence lines as well as the Er luminescence line, in all sets of diodes.The differences in the processing made no difference in the spectra that were obtained. A typical EL spectrum is shown in Figure 1-2

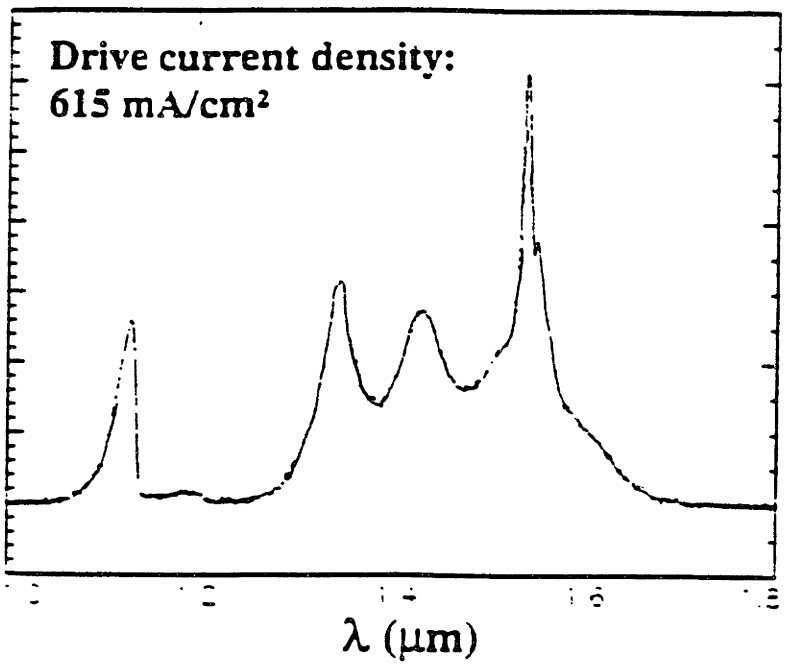

Figure 1-2: Typical EL spectrum of Si:Er LED's

The defect lines seen in the spectrum are the dislocation-related D lines, as shown by Sauer et al., which will be discussed later [10]. The primary thrust of this research was to determine the cause and location of the dislocations, and the processing steps involved. We believe that eliminating or even minimizing the dislocations would result in a higher signal from the Er^{3+} luminescence, and also a longer device lifetime. The ultimate goal of this device is high intensity room temperature light emission, for efficient use in optoelectronic systems.

1.2.2 Advances in Si:Er

Although there are indications of defects in the diodes that we have fabricated, Si:Er materials and devices have made significant improvements in the recent years. The diode will soon be directly integrated with a waveguide fabricated from polysilicon on the chip itself in our labs, shown in Figure 1-3. In order to make the most useful and efficient devices, the processing techniques and parameters must be optimized.

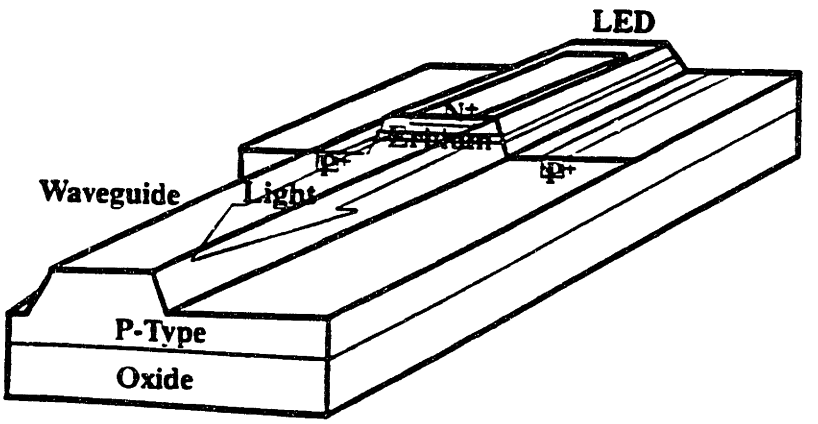

Figure 1-3: Cross section of a Si:Er LED integrated with a polysilicon waveguide

This result will require a higher percentage of optically active Er atoms, which we now estimate to be only 1% at room temperature. Once the preliminary devices are optimized, we will use the technology to fabricate lasers. Our silicon microphotonics system will be easily integratable into an IC package and will include parallel architectures with multiplexing, reduced clock speeds, and concurrent operations.

Chapter 2

Literature Review

2.1 Erbium-doped Silicon

Erbium doped silicon was first reported as an optoelectronic material by Ennen et al. only a few years ago, although using rare earth ions for light emission was not new [5]. Erbium is used in optical fibers for light amplification, and neodynium is used in YAG lasers for powerful light output. Rare earth ions (RE^{3+}, which are the optically active ion) in silicon all work the same way through excitation of electrons in the 4f shell. The radiative transition of interest in free rare earth ions are parity forbidden, but in host crystals the ions' 4f states become non-degenerate, allowing radiative processes to occur, due to the interaction between the Er and the host lattice. The number of $4f$ splittings that occur depends on the symmetry of the lattice site occupied by the rare earth ion, but examination of the luminescence of Er^{3+} in silicon has proven to be ambiguous in determining the definite lattice site that is being occupied. Tang et al. have shown, through photoluminescence studies of Si:Er, that some Er^{3+} ions are in the T_d symmetry states and that other ions are in sites of lower symmetry [11]. Because the $4f$ shell is well shielded from the lattice by the $5d$ shell, the transitions involved in the luminescence of Er ions in a silicon lattice are almost unaffected by outside perturbations [12].

Ennen et al. reported the sharp line photoluminescence of ion implanted Er^{3+} in silicon. The transitions shown in the spectra correspond to the weak crystal field split

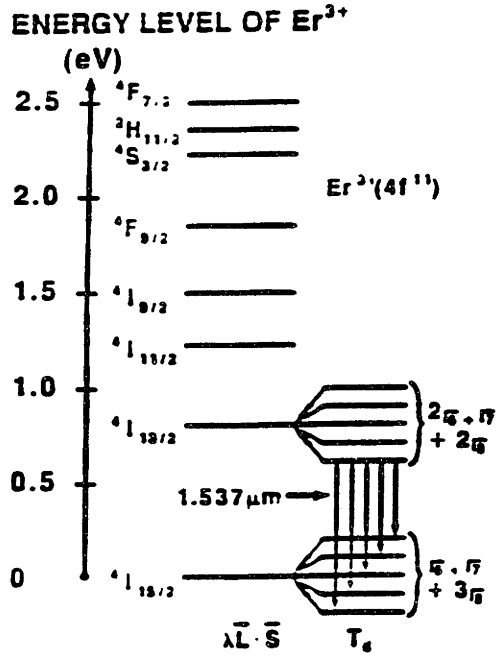

Figure 2-1: Er^{+3} $4f$ crystal field splitting

orbitals ${}^4I_{13/2} \rightarrow {}^4I_{15/2}$, showing luminescence at 1.54 μm [5]. The Er^{3+} field splitting is shown in Figure 2-1. The Er^{3+} ions are excited by pumping with laser light at an energy larger that the band gap of Si [5]. The exact mechanism of the excitation process is still unknown, but it is believed to be an impurity Auger process [9][5]. In these processes, carriers transfer their energy to the $4f$ electrons in the ground state through electron-hole recombination. The sharp line of the spectrum is attributed to the weak interactions of the Er^{3+} ions with the host lattice. In semiconductors, the spectral linewidth of Er^{3+} is $\Delta\lambda < 2\mathring{A}$ at 4K and $\Delta\lambda < 150\mathring{A}$ at room temperature. This sharp transition is useful in optoelectronic technology, in that it will ease laser technology at 1.54μm, because the linewidth of the laser increases with the linewidth of the excited medium [13] [6]. In addition to the sharp wavelength, Er devices, including lasers, will have an emission wavelength insensitive to the host material and temperature of operation [12]. The sharp temperature independent emission of Er in Si is probably the most useful property of Si:Er as an optoelectronic material.

2.1.1 Optical Properties of Si:Er

Thus far, all the Er doping that has been done in our labs has been through ion implantation. In order to achieve the depth of 1.5 μm and a concentration of $5X10^{17}cm^{-3}$ Er ions in silicon, high energy implants were needed. The implantation in itself brings about problems, which will be discussed later in this chapter. Erbium incorporation in silicon is limited by precipitation. These precipitates are Er-rich and appear as platelets of about 100-300A in thickness, and are probably $ErSi_2$, determined by the Er-Si phase diagram [7]. At 900°C, the solubility of Er in Si is about $1.3X10^{18}$ cm^{-3}, at which precipitation begins in both CZ and FZ silicon [7]. It was discovered early on that CZ silicon emission was more than 100 times higher than FZ silicon, the difference being the oxygen content in CZ silicon. The extra oxygen is important in the formation of optically active Er centers. Other light elements were also found to enhance the Er optical activity, especially C, N, and F. It is believed that impurity enhancement from highly electronegative ligands, such as C, N, and F, may be due to association with Er to form impurity complexes that cause the Er to change from an Er^{+2} state to an Er^{+3} state. Only the Er^{+3} state is optically active [8] [6]. The PL intensities as a function of the added implant are shown in Figure 2-2. In Cz silicon the ligands F, C, N, and O increase the Er luminescence intensity by a factor of 4. This shows that not all erbium ions are always contributing to the luminescence, and that a large number of the ions are optically inactive when Er is in the lattice without an added ligand [14].

The luminescence intensity of Si:Er, shown in Figure 2-3, is strongly temperature dependent, due to a number of different processes. Backtransfer may occur from the excited Er atoms to the lattice, creating more electron and hole pairs, phonons, or Auger excitation of free carriers, instead of a photon at 1.54μm. Competitive recombination paths, including phonon interaction and deep level defects, may also play a role in the decreased luminescence at room temperature. Annealing experiments show that optical activity of Er in Si depends also on the time and temperature of the anneal, with a 30 minute anneal at 900°C being optimal for Er luminescence [14].

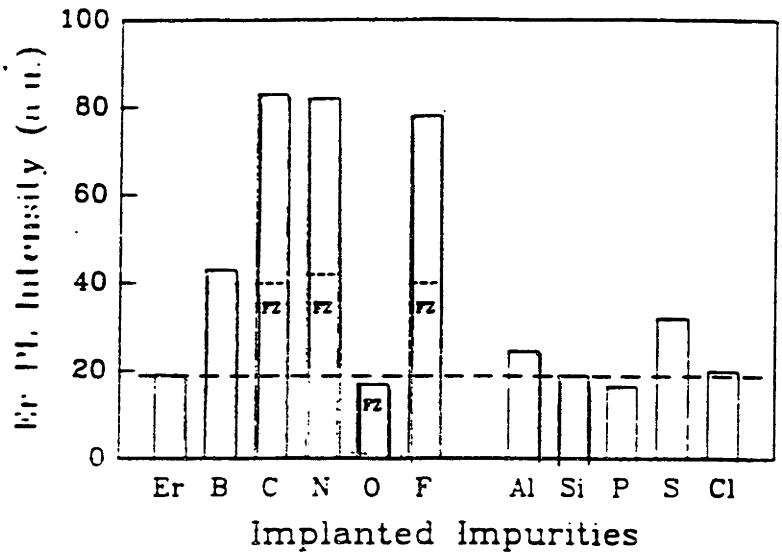

Figure 2-2: Impurity enhancement of PL signal of Si:Er [8]

Measurements show that only about 1% of the erbium is optically active at 300K, and that only about 10% of the Er is in a lattice configuration that can be optically active [14].

2.1.2 Electrical Properties of Si:Er

Studies of Si:Er by Benton et al. show that ion implanted Er in Si exhibits donor characteristics [15]. In Er doped p-type CZ silicon, annealed at 900°C for 30 minutes, the excess carrier concentration from the implanted Er increases linearly until a maximum is reached at an Er concentration of mear $10^{17}cm^{-3}$. This is shown in Figure 2-4 [15].

The optimum annealing temperature is found to be 900°C for maximum Er light emission, where the Er-O complexes are dominant [6]. At higher annealing temperatures, the Er-O complexes dissociate, and oxygen outdiffusion begins, resulting in a lower light output. Annealing time is important as well, as shown in Figure 2-5. The

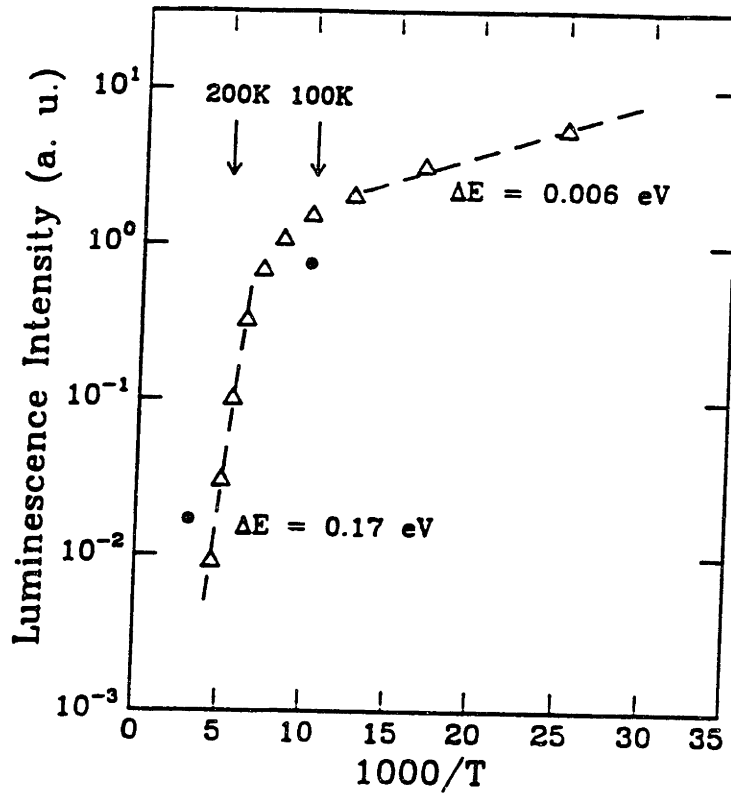

Figure 2-3: Temperature dependence of PL signal in Er doped CZ Si [8].

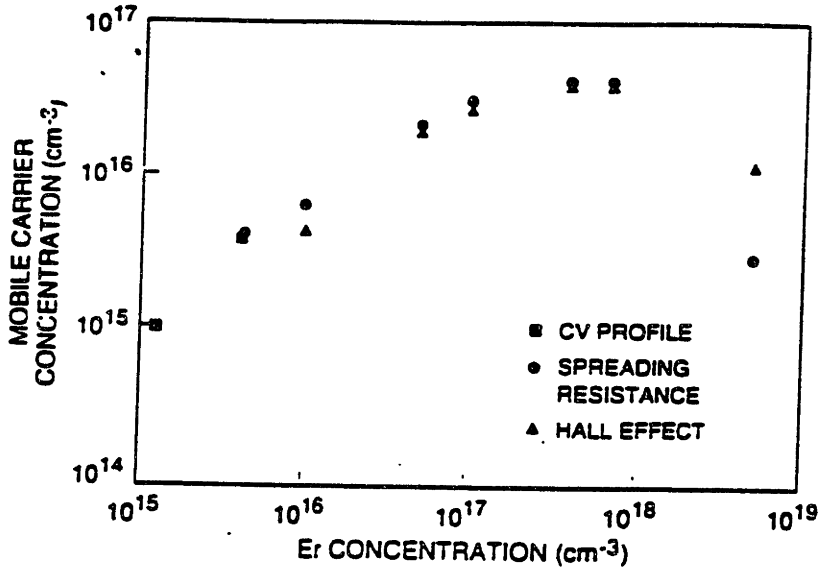

Figure 2-4: Free carrier concentrations as a function of implanted Er concentration [15].

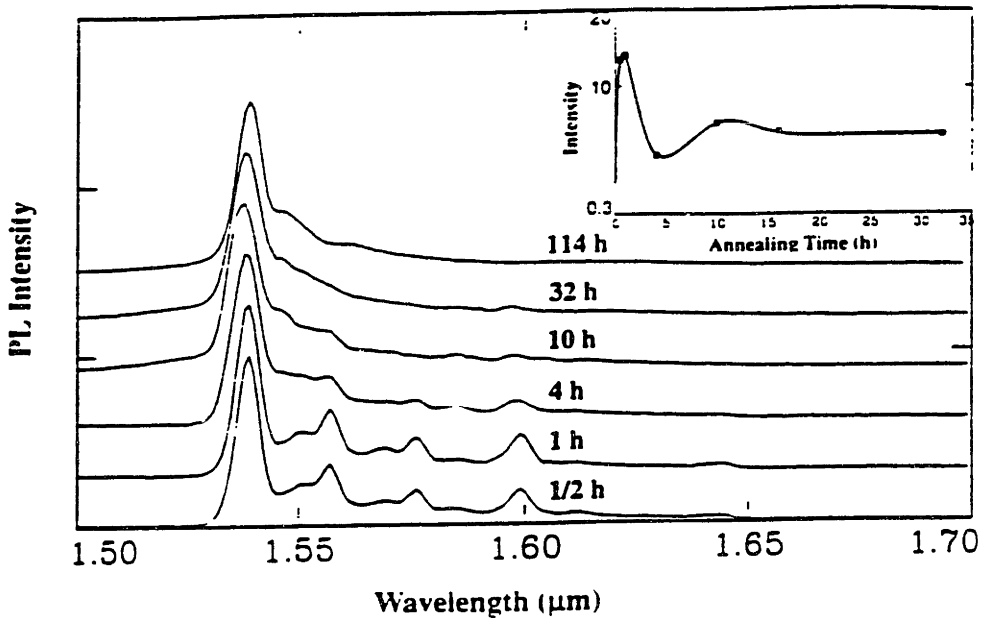

Figure 2-5: The effect of annealing time on the luminescence of Si:Er, with additional ligand O implant. The insert shows the PL intensity with time [6].

luminescence peak intensity is found after 30 minutes of annealing, after which the luminescence decreases by a factor of about 10. In preliminary studies, a 30 minute anneal at 900°C resulted in a sharp line spectra at 1.54μm, with no indication of residual defects in the Si lattice [6], shown in Figure 2-6.

It is not known the exact position of Er in the silicon lattice, but in later studies, Benton et al. showed that the luminescence comes from the Er defect complexes created by Er surrounded by six oxygen atoms. They also found that optical activity and electrical activity of Er in Si are not related, although the donor concentration is related to the PL intensity [16]. At high concentrations, the Er may start to occupy sites other than substitutional, in the form of Er^{3+} or other Er related complexes or precipitates, such as $ErSi_2$, which affect both the electrical and optical characteristics of Si:Er. This is consistent with the data from Tang et al., in which many different symmetry sites are seen in the PL spectra. The effect of electrical activity on the optical activity can also be seen in Figure 2-4, as the carrier concentration reaches a

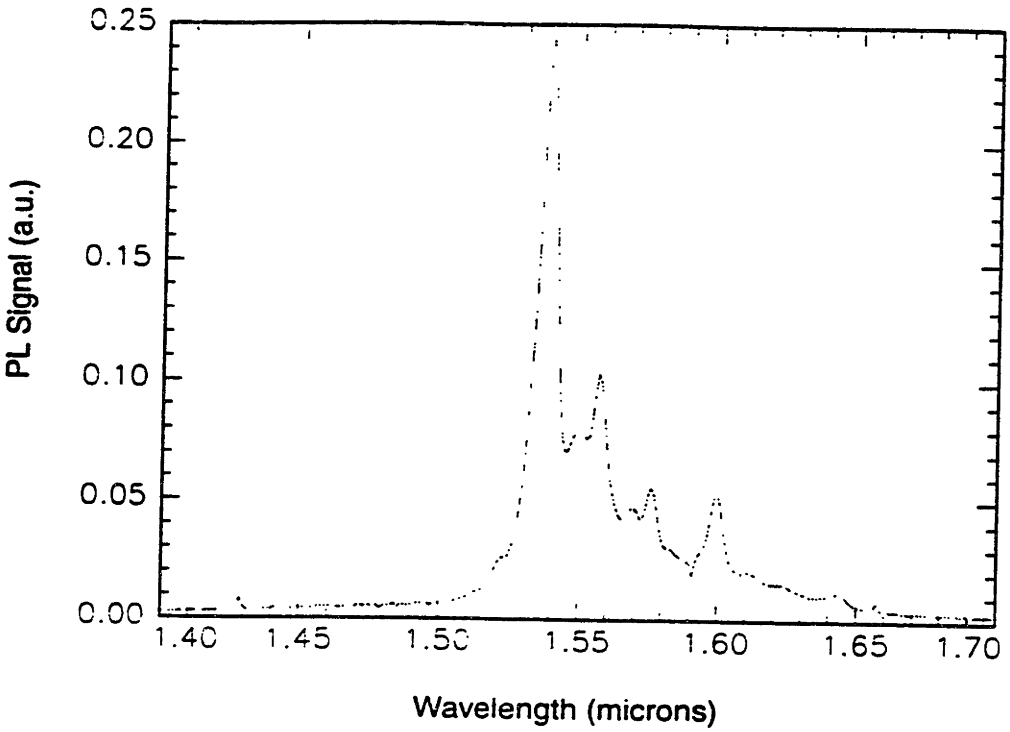

Figure 2-6: PL spectra of 30 minute anneal at 900°C of Si:Er with O implant.

maximum and then begins to fall at high concentrations, when the Er may begin to precipitate or associate [15]. The carrier concentration increase does not necessarily increase the PL signal of the Er, but may do so if more Er is ionized by defect complex formation into Er^{3+}. [16]

2.2 Dislocations in Silicon

Dislocations in silicon can act as recombination sites, trapping electrons and holes, and forcing them to recombine. Obviously this is detrimental to luminescence in our Si:Er LED's, in that the electrons and holes will recombine without diffusing to the Er layer. In ideal situations, the cores of dislocations are reconstructed. In reality, however, there are dangling bonds, which act as recombination sites, which are stabilized by either a hole or an electron, causing a trapping of charge [17] [18]. It has been suggested that the electronic transitions that are responsible for D-line luminescence occur in the dangling bonds of cores or at kinks, jogs or impurities at the

dislocation [19]. Photoluminescence studies in silicon show that dislocations produce characteristic spectra at wavelengths longer than the band edge. In 1976 Drozdov et al. reported that there are four lines that appear to be related to dislocations in silicon [10]. These four lines are labelled as D1 (1.53 μm), D2 (1.42 μm), D3 (1.33 μm), and D4 (1.24 μm). D1 and D2 are similar in structure and are associated with bound-to-bound transitions. They are related to point defects near the actual dislocation. D3 and D4 are also similar in structure and are due to free-to-bound transitions, directly related to the dislocations [10]. The four D-line spectra are said to be associated with "normal" deformation conditions, meaning stresses that are related to normal processing conditions, resulting in a equilibrium state for dislocations [10]. These dislocation lines correlate with the spectra seen in our Si:Er LED samples, because of the positions of the lines, showing D2 at 1.44μm, D3 at 1.33 μm, and D4 at 1.24 μm. The spectrum is shown in Figure 1-2, with the dislocation luminescence appearing at high drive current densities.

The D-lines are seen not only in plastically deformed silicon, but also in ion implanted silicon and cw laser annealed silicon. [10] [17] It has been seen that the broadening of the spectrum of the D-lines, is highly dependent on the processing conditions of the silicon, which influences the generation procedure of the dislocations [10]. In fact, Sauer et al. found that samples prepared exactly the same way never had the same intensity or structure of D-line luminescence [10]. Oxygen present in the lattice leads to line broadening for all of the D-line spectra [20], probably due to the interaction of the oxygen atoms with the dislocations [17].

Transition metals are important in D-line luminescence as well. The introduction of fast diffusing metals like copper, iron , and nickel in silicon has been the subject of much discussion and debate. One idea is that D-line luminescence is enhanced by metal contamination. In this argument, dislocations are present but their luminescence is not seen unless the sample is contaminated with a transition metal. The contamination causes the dislocations to luminesce strongly [19]. The opposing view is that transition metal contaminants actually passivate the D-line luminescence spectrum, and at high levels of contamination, the D-line luminescence is suppressed [21].

From these two differing viewpoints, it is clear that transition metal contaminants play a role in dislocation spectra. In the case of the Si:Er LED's, transition metals may be introduced through contaminated furnaces during annealing. It has been established, through lifetime measurements of Si wafers annealed in the MTL furnaces, that the furnaces are not contaminant free. The metals, which are fast diffusers, even at room temperature, can easily diffuse into the region damaged by ion implantation, and prevent complete recovvery of the damaged region. If there are impurities that diffuse into the damaged region, they could be the cause for dislocations to form.

Whatever the cause of the dislocations, they are an indication of poor quality material and devices. The primary objective of this research is to determine the step or steps involved in the device processing that are responsible for dislocation formation.

2.3 Ion Implantation in Silicon

Ion implantation is a useful method of incorporating dopants into silicon by bombarding the substrate with a high energy flux of ions. The advantage of ion implantation is a strong control over the number and placement of the dopants. A disadvantage of ion implantation is the damage high energy collisions will impart to the host lattice. Figure 2-7 illustrates the processes that occur during ion implantation. The high energy ion enters the lattice and undergoes a number of high energy collisions. Each collision imparts some kinetic energy to the atoms involved, which in turn gain some momentum, and may cause even more collisions to occur. A single high energy atom may cause the displacement of hundreds of lattice atoms [22]. When many high energy ions bombard the substrate, lattice damage occurs, resulting in defects and amorphization. The disordered region created by each incident ion contains a central core in which the defect density is very high, containing vacancies, divacancies, Frenkel defects, and dislocations [23]. As more and more ions are implanted, the defective regions begin to overlap, and this causes an amorphous layer to form. To form an amorphous layer, the critical dose (per cm^{-2}) must be exceeded. In silicon,

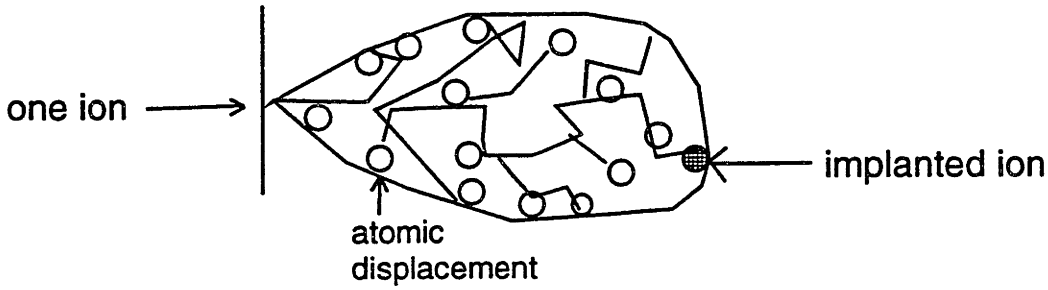

Figure 2-7: A representation of damage introduced by an ion in ion implantation

this number is about $10^{14} cm^{-2}$ for medium to heavy ions [24].

Much of the damage in the lattice caused by ion implantation, be it defects or amorphization, can be annealed out at elevated temperatures, but residual damage will still exist in the form of dislocations and point defect clusters, even after annealing. The damage caused by implantation has a detrimental effect on the minority carrier lifetime and mobility, both of which are important for device performance. Annealing will "fix" some of the damage, but with high dose implants, full carrier activation is very difficult to achieve [23].

In amorphous silicon, regrowth occurs by solid phase epitaxy (SPE). The regrowth begins at the amorphous-crystalline interface, and grows upward toward the surface, at a velocity that is set by the dopant, doping concentration, and crystal orientation.

Impurities in the lattice can either slow down or speed up the regrowth process. Impurities such as O, C, or N slow down growth, probably because of their affinity to dangling silicon bonds [25], while impurities such as B, P or As speed up the growth rate. As the amorphous layer recrystallizes, dislocations form in and around the implanted region [23]. Phosphorus can amorphize silicon at doses of mid-10^{14} cm^{-2}, and annealing at temperatures around 950C results in a honeycomb-type dislocation network. Arsenic, a heavy implantation ion, has a critical dose of about $2x10^{14}cm^{-2}$. Annealing will cause winding dislocation loops and half loops of edge dislocations to form [24]. In our junction implantation steps of phosphorus or arsenic, the critical dose was exceeded, but the Er implantation did not reach the critical dose. It is not uncommon to generate dislocations in ion implanted materials, but we must consider the effect that residual damage and dislocations will have on the devices.

2.3.1 High Energy Er Implantation

MeV implantation has different annealing characteristics than low energy implantation, because the formation of defects depends on the stopping processes in high energy implants. The damage that is created is predominant at the end of the projected range of the implant, due to the nuclear stopping processes involved [26].

A buried layer of Er ions can be formed using a high energy implant of Er. In our diodes, we used a 4.5 MeV implant, but with the dose low enough so as not to cause amorphization. With a buried layer of high concentration comes a buried defect layer that is formed near the peak of the implanted region. Even under high temperature annealing conditions, the defect layer that is formed is much more stable than other ion implantation damaged layers because of the depth of the defective layer. Defects formed by using implantation energies higher than 1MeV are so far from the surface, that annihilation at sinks is difficult [27]. In the case of dual high energy implants, as we have done with our Si:Er diodes, more damage is induced and the result is extended defects after annealing [24].

Studies of Er implanted in Si were done by Eaglesham et al. and concentrate on the microstructure of the implanted layers [7]. They found that for implants of

500keV Er in CZ Si at a peak concentration of $6.6x10^{18}cm^{-3}$ at doses below the threshold for amorphization, defects took the form of Er-rich platelets. The platelets had precipitated around the peak of the Er implant,and resembled $ErSi_2$ in structure. In higher dose implants, they found that amorphization occurs. During the anneal, they found that the same precipates form, but also that the recrystallization is highly defective, including stacking faults and twins, extending up to the surface. They concluded that Er has a high tendency to segregate during solid phase epitaxy [7]. Another study on erbium implantation in silicon by Polman et. al. shows that 900°C annealing causes the formation of twins at and near the peak implantation region. The dislocation densities they found were so high that they concluded that only carriers generated in the immediate vicinity of the Er ions would actually cause Er excitation [28].

High energy implantation is often the cause of damage and dislocations because the defect layer is far from the surface, which acts as a sink to anneal out dislocations. The use of 4.5 MeV implantation in Si:Er LED's is probably an important factor in the dislocation formation.

2.3.2 Effects of Oxygen on Implantation Damage

Interactions between defects and existing or implanted oxygen can be very complicated [27]. High temperature annealing induces out-diffusion of O in CZ silicon toward the surface. As the oxygen is diffusing, it interacts with the residual defects produced by the implantation damage [27]. Oxygen atoms in silicon that interact with high energy ion implants can introduce buried defects in the substrate, as discussed in the previous section. The main residual defects of oxygen interactions are dislocation loops and networks, which may be caused by oxygen atoms becoming trapped in defect bands during early annealing. As the annealing continues, precipitates form (such as SiO_x), which continue to grow as more oxygen atoms interact with the dislocations and become trapped [27]. Oxygen also interacts with the vacancies in the implanted layer. During implantation, a vacancy-rich region before the peak range and an interstitial-rich region beyond the peak range are formed. Oxygen

atoms combine with the vacancy related point defects and form complexes. During high temperature anneals, the complexes diffuse into the damaged regions, and cause dislocation growth, by providing dislocation cores [27].

In the Si:Er LED's, the deep implants of Er and O occur at high energies, which in itself form a buried layer of defects near the peak range of the implantation. The deep defects are very difficult to anneal away. The oxygen may interact with the defects present from implantation, and may complicate the problem of understanding the responsible steps in dislocation formation. All the possibilities should be accounted for in the determination of the responsible steps in the dislocation formation in the LED's.

Chapter 3

Scanning Electron Microscopy

3.1 Scanning Electron Microscopy Fundamentals

Scanning electron microscopy has proven to be an effective tool in the characterization of semiconductors, especially for studying methods which use the generation of excess carriers in the material [29]. The SEM used in this research is the JOEL 6400, with normal SEM capabilities to 300,000X and 40kV. The system also includes an EDX attachment from PGT, and a cold stage for low temperature measurements, from Oxford, for cathodoluminescence and EBIC, both of which will be discussed further. In order to understand the experimental techniques used, it is important to understand how the electron beam from the microscope interacts with a semiconductor. The scattering mechanisms when the electron impinges on the surface of a semiconductor can be divided into elastic and inelastic processes [30]. Elastic scattering of impinging electrons by the atoms causes high energy backscattered electrons to be produced and used in the atomic number contrast options of the SEM. Inelastic scattering can be used in secondary electron emission imaging, generation of electron and hole pairs, characteristic x-ray spectra. and Auger electron production [31]. Scanning electron microscopy and the associated methods are useful, nondestructive techniques, and are used effectively in this research as a characterization tool.

3.2 Electron Hole Generation and Range

The incident electron's original trajectory is much changed as it travels through the semiconductor, due to various scattering events. Each incident electron has a very high energy, on the order of 10^3 eV, and the collisions of the high energy electrons form many lower energy electron- hole pairs in a cloud-like formation , which is sometimes called the generation droplet [30]. However, all of the energy of each incident electron does not create electron hole pairs, because some of the energy is backscattered and some more is converted to heat. For any semiconductor material, there is an average value E_{eh} of energy needed to create an electron hole pair, that takes into account the energy losses due to backscattering and heat loss. For silicon, this value is 3.6eV, which has been developed from a phenomenological model by Klein [32].

3.2.1 Electron range

As a result of the scattering and heat losses, there have been many models to determine the exact range of the electrons in the material. The range of the electron penetration can be given as:

$$R_e = (k/\rho)E_b^{\alpha} \tag{3.1}$$

Where E_b is the beam voltage, ρ is the density of the material, k depends on the atomic number of the material, Z, and α depends on the atomic number and the electron beam energy. An evaluation of these constants in silicon for beam voltages of 0-40KeV has been determined by Kanaya and Okayama, and was found to agree well with most experimental data. According to their research, the range R_e is given by:

$$R_e = (0.0276A/\rho Z^{0.889})E_b^{1.67} \tag{3.2}$$

In this equation, A is the atomic weight in g/mol. The electron range is shown below for various semiconductor materials in Figure 3-1.

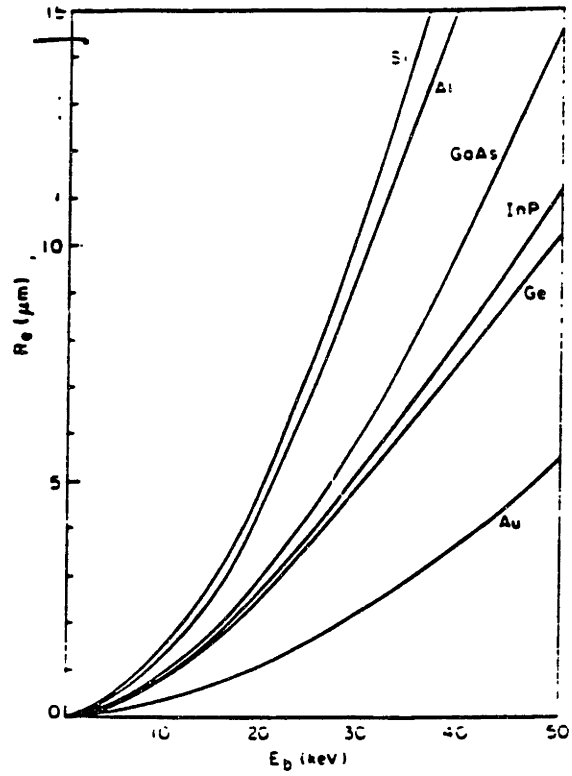

Figure 3-1: Electron range for semiconductors as a function of accelerating voltage from the Kanaya-Okayama model [27].

3.2.2 Generation Volume

The generation droplet created by the carriers as they travel through the semiconductor varies as the material does. In heavy materials, the generation volume is hemispherical, while for materials with lower atomic numbers, the generation volume changes from spherical to pear shaped. This is shown in Figure 3-2. The generation volume can be mathematically modeled using a normalized distribution function $< g >$.

$$g(r,z) =< g > (EI_b(1-f)/E_{eh}q) \tag{3.3}$$

Where g(r.z) is in units of carrier pairs/cm^{3}sec. I_b is the electron beam current, and f is the fraction of the electron beam energy that is reflected from the sample. For silicon, f=0.08, and is a small numerical correction factor. As mentioned before, E_{eh} is the energy needed to create an electron hole pair in a semiconductor, and in silicon, E_{eh}=3.6eV [30]. The normalized function $< g >$ has been determined experimentally

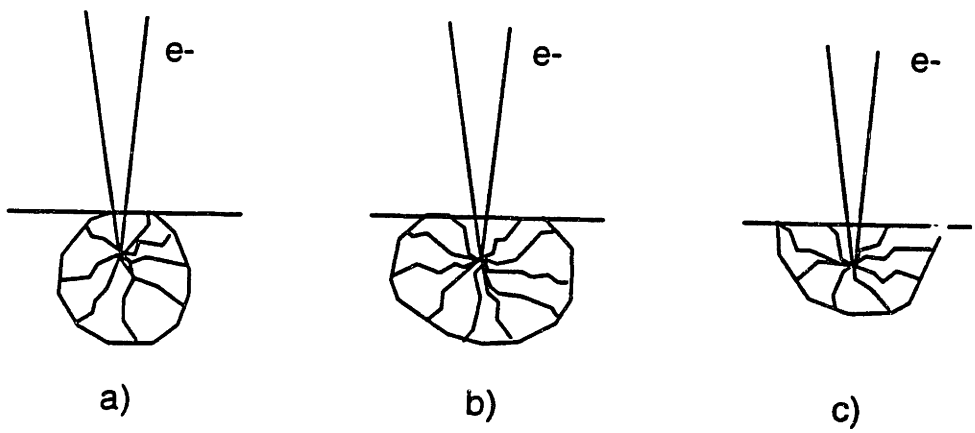

Figure 3-2: Generation volume for a)low atomic number materials b)15<Z<40 and c)large atomic number materials.

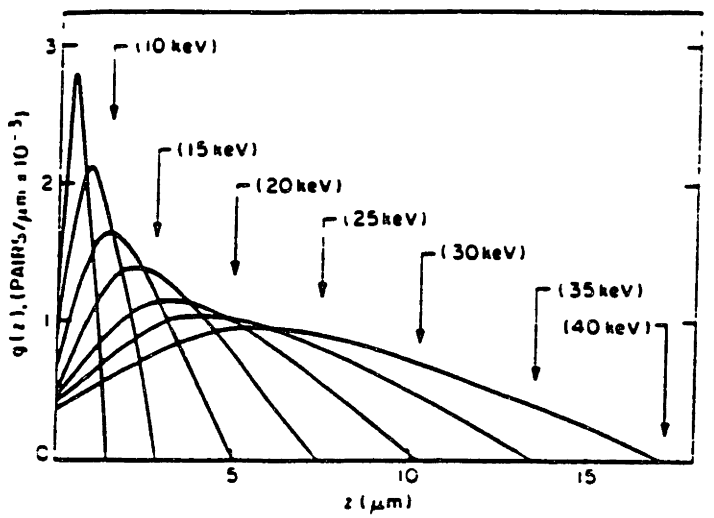

Figure 3-3: Everhart and Hoff's determination of the carrier generation function with respect to the distance the electrons will travel in silicon [27].

for silicon [33], and has a radial component and a longitudinal component. The radial component, g(r), is a gaussian profile, and the longitudinal component, g(z), whose values are important in this research, is given as:

$$g(z) = 0.6 + 6.21z - 12.40z^2 + 5.69z^3 \tag{3.4}$$

where z is given in terms of R_e, the electron range in the material. The generation function depth for different accelerating voltages is given in Figure 3-3. In future calculations and discussions, the peak of the generation volume for different accelerating voltages is useful to know. If the derivative of g(z) is taken and the maximum calculated, with $z = x/R_e$, where x is the peak depth of the generation droplet, a value can be calculated for x. The results are given in Table 3-1.

With these fundamental terminologies of scanning electron microscopy, the methods used in this research can be better understood. Primarily, the SEM is used in

Table 3.1: Calculated Values of Peak Generation Volume

kV	Peak of Generation Volume (microns)	Range(microns)
10	0.58	1.8
15	0.96	3.0
20	1.3	4.0
25	2.25	7.0
30	3.5	11.0
35	4.8	15.0
40	5.5	17.0

this research to do cathodoluminescence (CL) measurements and electron beam induced current (EBIC) measurements. Both of these methods are important tools in the characterization of semiconductors, and can provide information on structural defects in the material.

3.3 Electron Beam Induced Current

3.3.1 EBIC Theory

Electron beam induced current is an SEM measurement method in which the sample itself is the detector of electronic charge [30]. Charge carriers are generated from the impinging electron beam and they move in response to the depletion region of the semiconductor to produce a collectible signal. It follows that to use EBIC as a characterization tool, there must be either a Schottky barrier or a p-n junction in the sample to provide the depletion width. A schematic representation of EBIC is shown in Figure 3-4

In a p-type semiconductor, for example, the minority carriers, the electrons, generated by the impinging high energy electron beam, diffuse to the junction, and are swept across it by the electric field induced by the depletion region. The electrons produce a current which is collected on the surface of the semiconductor. This current is what is collected from all scanned points of the sample and viewed on the screen of the SEM. The opposite occurs for an n-type sample, and the holes diffuse to the junction to provide the collected current.

In the case of a defect level in the semiconductor, a recombination event occurs. The recombination events, which can be caused by point, line and crystallographic defects, can be imaged with EBIC as contrast sources in the image [30]. The defect level reduces the lifetime of the minority carrier, and the defect will appear on the SEM screen as an area of less collected charge because the carriers that recombine at the defect will not be collected at the junction. In the setup that is used in this experimental work, the defects should be seen as dark areas in a bright field [30]. A

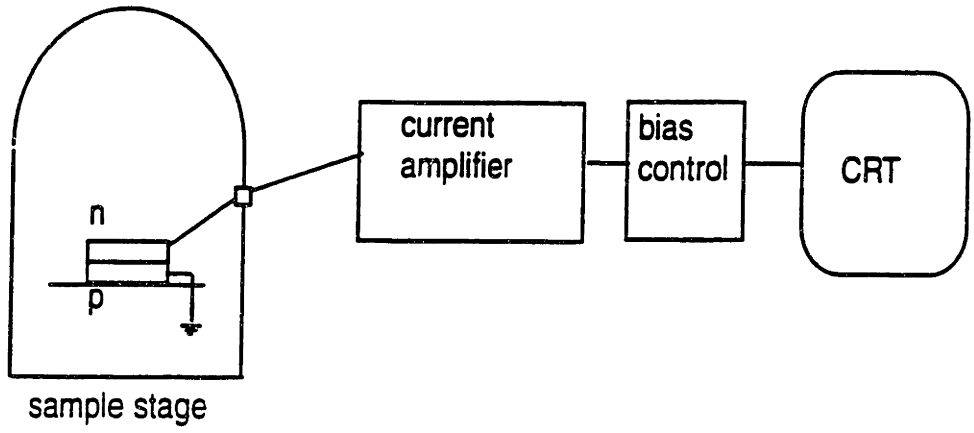

Figure 3-4: A schematic of the EBIC mode of the SEM

schematic of an EBIC image, showing a defect level and contrast is shown in Figure 3-5. The imaging of the defects depends on the resolution that can be achieved with the accelerating voltage that is being used [34]. As the beam energy increases, the resolution and contrast of defects that can be imaged decreases because of the increased volume of carriers produced in the sample [34].

EBIC can also be performed at low temperatures, and will usually show an increase in contrast due to the temperature sensitivity of the measurement. The Fermi level in a p-type semiconductor varies as:

$$E_i - E_f = kTln(N_A/n_i) \tag{3.5}$$

and in an n-type semiconductor.

$$E_F - E_i = kTln(N_D/n_i) \tag{3.6}$$

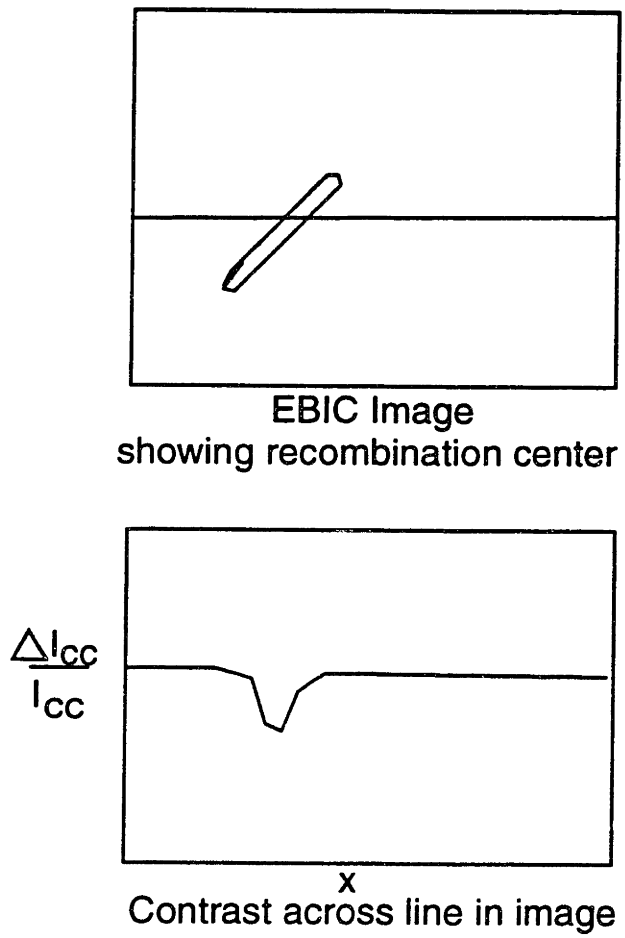

Figure 3-5: An EBIC image, showing collected charge and defect level.

As the temperature decreases, the Fermi levels in the semiconductor change linearly, and as a result, defect levels near the conduction band are filled. At the defect levels in the gap, either electrons or holes can be trapped. depending on where the Fermi level is in the gap. If the defect level is above the Fermi level, it will trap electrons, if it is below, it will trap holes. The capture rate of electrons and holes are determined by the capture cross sections. If the capture cross section of a hole, σ_p, is much less than the capture cross section of the electron σ_n, recombination will be limited by the availibility of empty electron traps. As the defect levels are emptied in this example, depending on the temperature, the states will capture an electron, causing enhanced contrast to be seen in an EBIC image.

3.3.2 Sample Configurations

To use EBIC, as mentioned before, there must be a depletion width in the sample. The sample may have either a Schottky barrier or a pn junction. The field provided by the depletion region causes the charge to be swept across it and collected at the surface. Various sample configurations are shown in Figure 3-6. The junction can be parallel to the beam, as in Figure 3-6a, or perpendicular to the beam, as in Figure 3.6b. The schematic shown in Figure 3-5 is the imaging that will occur in the case of Figure 3-6b. In the case of Figure 3-6a, the EBIC image can be compared to a one-dimensional image of the collection at the pn junction itself.

3.3.3 Charge Collection Efficiency

In EBIC,the sample must be connected carefully to the sample stage. As shown in Figure 3-4, contact to an ammeter or the SEM CRT through a current amplifier must be made through both the p and n sides of the sample. This was done using a gold wire bonded to the top contact of the diode, and the sample stage was connected to the bottom contact of the diode. The current collected is them connected to the CRT, where it is seen as an image. If the collected current is instead connected to an ammeter, the collected charge can be quantitatively read. This value can

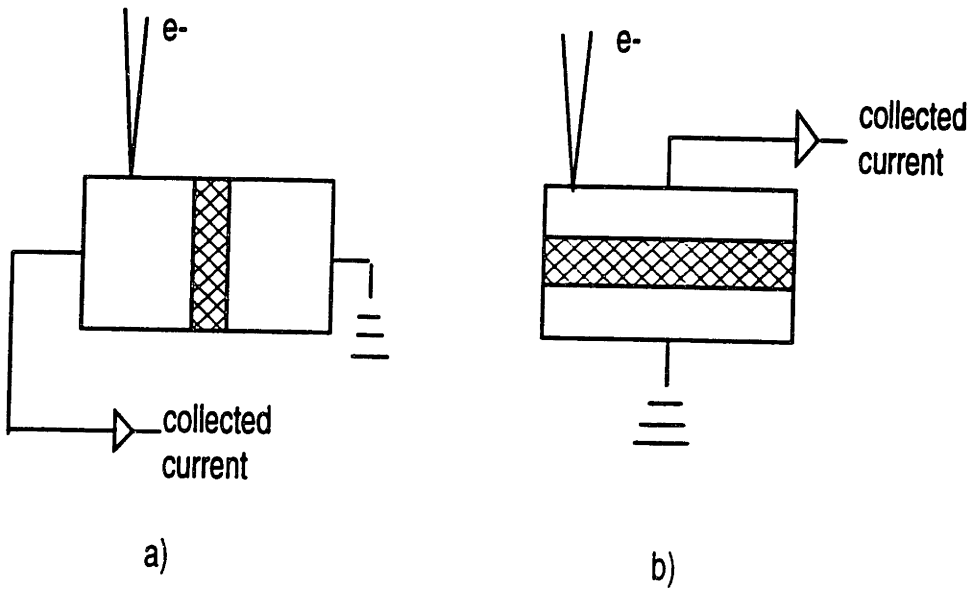

Figure 3-6: EBIC sample configurations, a) parallel to the beam, and b)perpendicular to the beam

This value can give important information about the charge collection efficiency of the diode, and subsequently about the quality of the material.

The charge collection efficiency η is given as:

$$\eta = I_{cc}/I_g \tag{3.7}$$

I_{cc} is the collected current, measured by the ammeter, and I_g is the maximum current generated with the given beam conditions. I_g can be given as : [30]

$$I_g = (I_b E_b (1 - f))/E_{eh} \tag{3.8}$$

High collection efficiencies indicate low levels of recombination sites, because the collection efficiency is directly related to the carrier diffusion length. As the beam energy increases, the depth of carriers increases as well. If the carrier diffusion length is short, then the deep carriers will not be able to diffuse to the surface to be collected

as charge, resulting in a decrease in the EBIC efficiency with increasing acceleration voltage.

Qualitative and quantitative EBIC can be very useful in determining the defects in semiconductor materials, and are a large part of this research.

3.4 Cathodoluminescence

Cathodoluminescence (CL) is the emission of light from excitation by an electron beam of the SEM. CL is useful in that it gives both spatial and spectroscopic information. The equipment used in CL can be attached to an SEM and is commercially available from Oxford Instruments. It consists of a parabolic mirror above the sample where the light is focused at the focal point, into a light pipe, which leads to the spectrometer, which is computer controlled. To achieve high resolution CL spectra for Si:Er materials, high beam currents must be used, on the order of 1μA, which is the limit of our SEM. A schematic of the CL equipment is shown in Figure 3-7. The cold stage can be used for CL as well and is useful in eliminating non-radiative recombination events which dominate at elevated temperatures. The spectra obtained by CL is similar to that of photoluminescence (PL) or electroluminescence (EL). However, in CL a local injection volume of carriers is created by the beam, as opposed to the whole junction injection in EL and a light spot injection in PL. The electron beam creates many more carriers, each electron producing on the order of 1000 electron hole pairs, making the signal much higher. The variation of the carrier generation range of impinging electrons with accelerating voltage can be used to create a depth profile of the luminescence centers. As the accelerating voltage is increased, carriers come from deeper regions in the semiconductor, yielding a signal maximum at the origin of the luminescence. Then the CL signals can be normalized for comparison, with reference to the accelerating voltage and beam current, using the simple equation:

$$Normalized\ Signal = (signal)/I_g \tag{3.9}$$

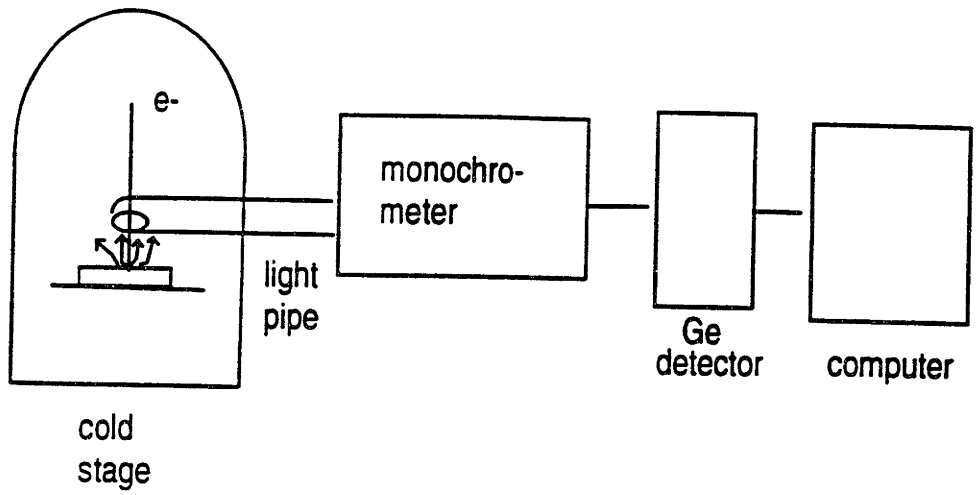

Figure 3-7: The schematic representation of the SEM with cathodoluminescence attachments

3.4.1 Intrinsic and Extrinsic CL

Cathodoluminescence can be broken down into two different types, intrinsic and extrinsic spectra. Intrinsic spectra is due to recombination across the band gap of the semiconductor only. Any changes that would affect the size of the band gap, such as temperature for example, can be monitored by the intrinsic CL spectra. In direct bandgap materials, this is the dominant form of radiative emission. In the case of silicon, an indirect bandgap material, phonons play a major role in the nonradiative recombination, resulting in low bandgap emission relative to the defect level emissions [31].

An intrinsic emission in silicon is the exciton spectrum, seen at low temperatures, which can be a measure of the quality of the material. At low temperatures, the electron and hole pair form a bound state, which is called the exciton, in which the electron in the conduction band and the hole in the valence band move together correspondingly, but in different bands. When this happens, and the pair recombines,

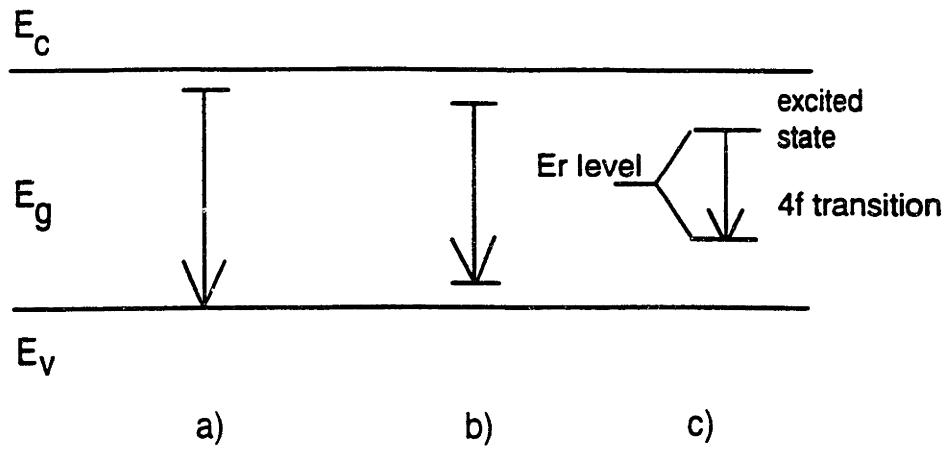

Figure 3-8: The different emission mechanisms for CL. a) Free or bound exciton b)donor-acceptor pair c)rare-earth ion

the energy levels of that pair are closer together than the width of the band gap, due to the Columbic attraction [31].

Extrinsic CL spectra are the emission from defects or impurities, schematically shown in Figure 3-8 . The first transition shown is the free or bound exciton line, seen at low temperatures. The second transition is an example of a donor acceptor pair, which produces extrinsic CL, and the third is the radiative decay associated with rare-earth ions, such as erbium [31]. Each spectral line energy is characteristic of a particular defect, usually found in the literature. Dislocations in silicon produce both shallow and deep level states in the gap, and their spectra are characteristically defined, as discussed in chapter 2. CL is useful in spectroscopic measurements of radiative recombination sites which emit photons which then can be detected.

3.4.2 Low temperature CL

The band gap of a semiconductor is a function of temperature, and contracts at higher temperatures, affecting the emission spectra in CL. The changes in band gap with temperature can be monitored by the changes in spectra. Additionally, from Debye theory it is known that at lower temperatures, there are fewer phonons, which indicate a lower loss to non-radiative recombination. In addition to the changes at low temperatures, it is important to remember that the Er luminescence is temperature independent. At near liquid helium temperature, the CL spectrum is much sharper and more intense than at higher temperatures, which is very useful in this research.

Spectroscopic low temperature CL can determine the nature of the defects and their causes, through the sharp spectral lines. For Si, the CL spectrum of various defects have been tabulated, which are very useful in understanding the spectra that are taken in the Si:Er materials [10].

The two methods of characterization described in this chapter are the basis of this thesis. Using EBIC and CL, the source and characteristics of the defects in the Si:Er light emitting diodes will be understood, and suggestions for improvements will be made.

Chapter 4

Experimental Results and Discussion

4.1 Dopant Characterization of Er

From the studies of Benton et al. it is believed that Er is a donor in silicon, and that the dissolved erbium is responsible for the luminescence properties that are seen. The Er luminesces through the $4f$ transition, by complex formation such as Er-O which enhances the light output, by forming the optically active Er^{3+} [14] [16]. Although Benton states that the donor concentration is not responsible for the luminescence by excitation processes, it is correlated to the luminescence intensity, but the exact relationship is unknown [16]. For optimal luminescence, the concentration of optically active Er ions should be maximized in the lattice, but the donor characteristics of Er are important to understand in order to optimize device parameters.

To be certain that the Er in our samples is indeed exhibiting donor characteristics, a C-V measurement was done, using a packaged Si:Er LED, connected to a C-V profiler. The LED has a background dopant concentration [B]= $10^{16}cm^{-3}$, and the junction depth is 0.4μm. The C-V plot shown in Figure 4-1 shows the dopant concentration on the p-side of the junction. The depletion width at zero bias is about 0.5 μm, and the background concentration that was measured is about $8x10^{15}cm^{-3}$.The

measured value agrees with calculated values, using the following equation:

$$W = [(2K_s e_o/q)V_{bi}(N_A + N_D/N_A N_D)]^{1/2} \tag{4.1}$$

and

$$V_{bi} = (kT/q)ln[N_A N_D/n_i^2] \tag{4.2}$$

where $N_A = 10^{16}$ cm^{-3} and $N_D = 10^{20}$ cm^{-3}

The calculated depletion width at zero bias is 0.4μm.

Our measurements show a compensation of the p-type dopant which peaks at about 1.5 μm, consistent with the doping peak of the Er implant. The compensation, however is very small, reducing the p-type dopant concentration only to $1x10^{15}cm^{-3}$, as compared with the concentration of Er implanted, which was $5x10^{17}cm^{-3}$. The reference diode, containing only the junction, but no Er or O, did not exhibit the compensation effect. Because the compensation is seen at all, we can be sure that the Er in the LED is acting as a donor in the silicon, even though the electrical activity may be very low. The concentration of Er that is measured in the C-V plot is approximately 1% of the total implanted concentration, which is in agreement with studies from Benton et al. [16]. Another possibility of the low measured concentration of carriers may be that the Er dissolved into the silicon at 900°C is limited by precipitation, and the measurement is the amount of Er left in solution, which is on the order of $10^{16}cm^{-3}$ [6].

The measurement indicates that there is carrier compensation, from which we can conclude that Er is indeed a donor in Si. A typical Si:Er LED I-V curve is shown in Figure 4-2, showing a turn on voltage of 0.5 V and normal diode behavior. However, the background dopant level of the Er LED is lower than the reference diode, which may indicate that the Er is diffusing farther into the substrate than expected. The diffusion constant of Er at 900°C is $10^{-16}cm^2/sec$, giving a diffusion length of 160$\mathring{A}$ after a 30 minute anneal. This is a very small amount of diffusion, which would not result in the background dopant difference in the LED. The carrier compensation of the background dopant is probably due to the oxygen content in the LED, or other

defects.

4.2 EBIC

The three sets of fabricated LED's were imaged with EBIC, at both room temperature and liquid helium temperatures in the cold stage attachment. Imaging at lower temperatures did not give any extra information. The estimated dislocation density from etch pit counts is on the order of $10^8 cm^{-2}$, discussed later in this chapter. At such high densities, the distance between the dislocations is less than the size of the generation droplet of the beam, resulting in insufficient contrast at single dislocations. The diodes were gold wire bonded and then soldered to a pin connector which was connected inside the SEM chamber and then through a port to either the CRT for imaging or an ammeter for current measurements, as seen in Figure 3-4.

4.2.1 EBIC Images

At low magnification, the whole die could be imaged, to check for electrical isolation, in which the bright regions are areas of high current collection and the dark areas are regions of low current collection. The reference diodes, which were not doped with Er and O were isolated, as were the diodes that had been implanted after a mask step in which the mask covered the whole wafer except the mesas, where the Er was to be implanted (diode set C-2). An image of the electrically connected diodes is shown in Figure 4-3, and an image of an isolated reference diode is shown in Figure 4-4.

The electrical connection was further investigated, and is thought to be a thin Er layer across the substrate. Evidence for this conclusion will be discussed in a later section.

At higher magnification, imaging dislocations or other defects was attempted at temperatures between 20K and 300K. There was no contrast in any images until currents greater than 10nA were used. At low temperatures, (< 100K) the current needed to image any contrast was higher, on the order of 20nA. SEM micrographs showing both the EBIC image and the secondary electron image are shown in Figure

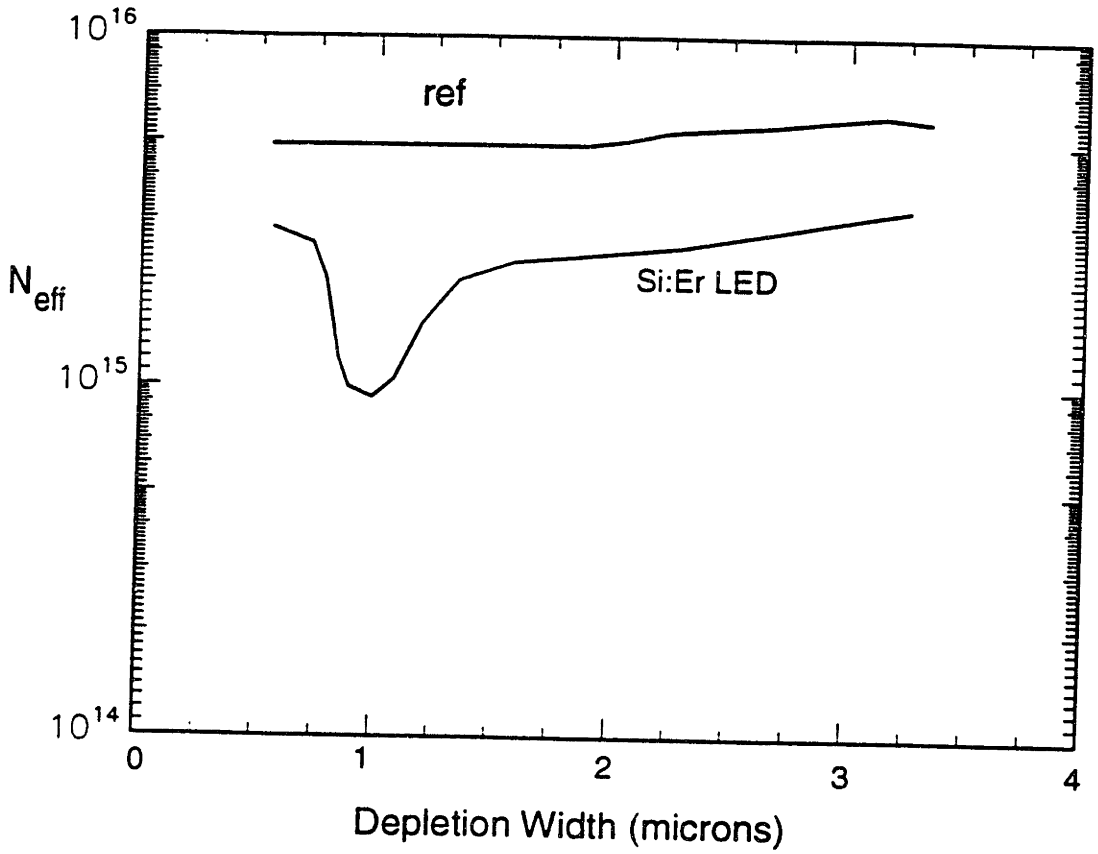

Figure 4-1: C-V measurement of Si:Er LED, showing Effective carriers vs. Depletion region depth.

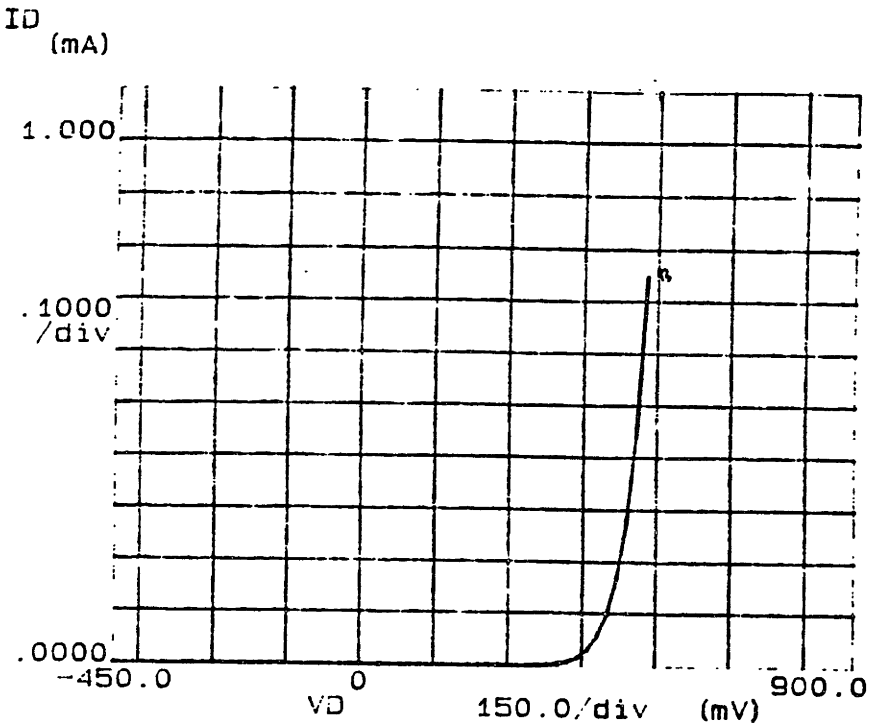

Figure 4-2: I-V curve for Si:Er LED.

4-5. The very dark spots on the EBIC image are seen on the SEI as dust or another impurity on the surface, but the fuzzy darker areas are EBIC contrasts. From the accelerating voltage used, using the graph in Figure 3-1, we can determine that the beam is creating carriers at a range of 1.5μm of the sample. Increasing the probe current to relatively high values, (the usual imaging currents are on the order of 0.5nA), can cause changes in the recombination lifetimes of carriers at the defects, due to increased injection levels, which is the reason that the contrast can be seen at some currents but not others [30]. The areas of contrast seen in the EBIC images may be dislocations or other defects, but from their shape and from the accelerating voltage at which they are most visible, it is more believable that they are caused by the variations in the passivating oxide layers. The contrast is seen at both low accelerating voltages of about 5 kV and higher accelerating voltages of 20kV . The oxide will absorb some of the carriers before they reach the surface of the sample, and in places of thicker oxide, the number of carriers being absorbed will be higher, causing contrast in the image. Another effect of the oxide is charging, which may also

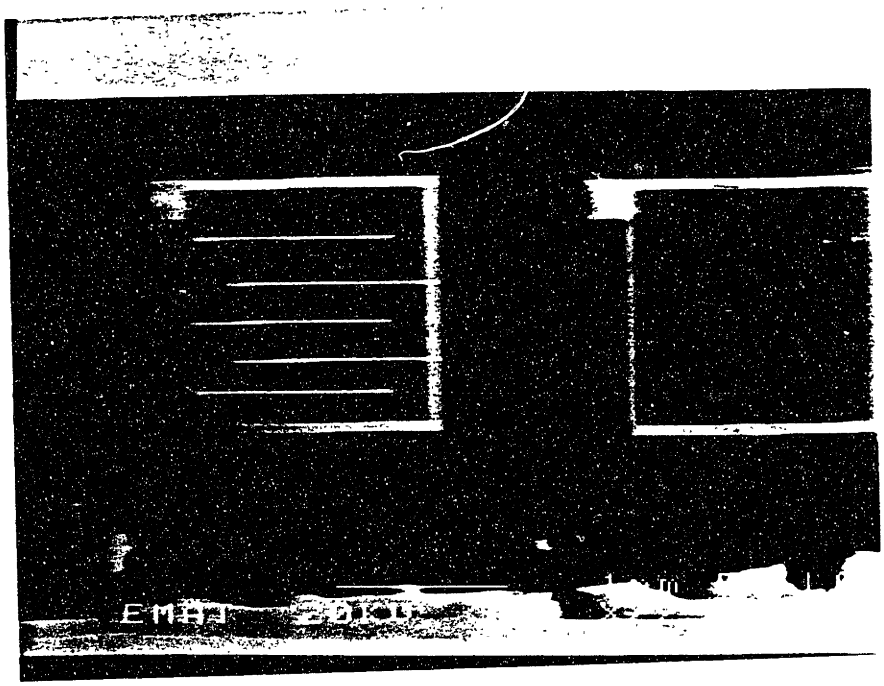

Figure 4-3: Si:Er LED EBIC image, showing electrical connection through the substrate and a schematic illustrating the effect. Only the diode on the right is electrically connected.

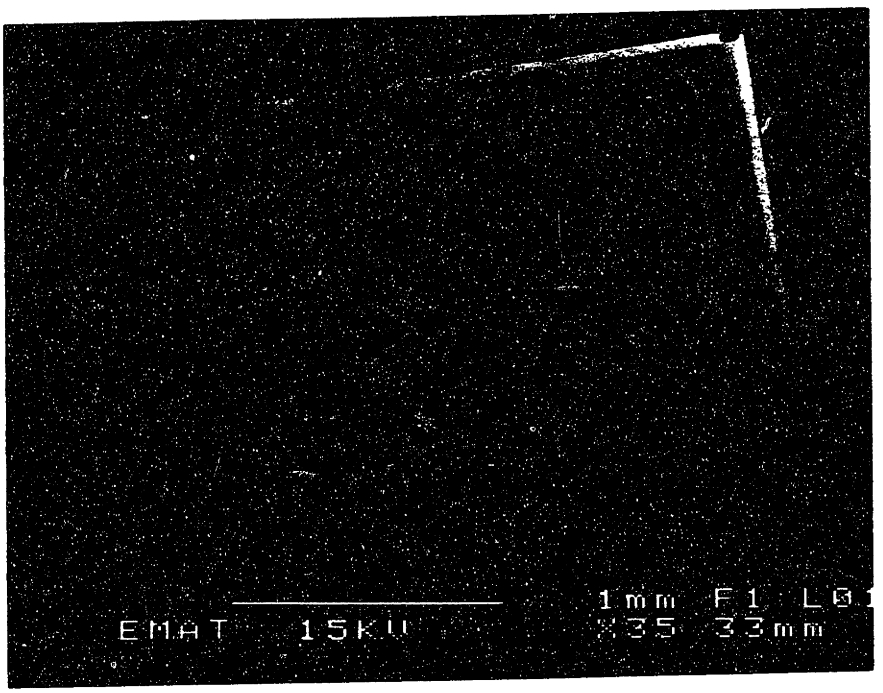

Figure 4-4: EBIC image of reference diode. The processing of this diode was the same as the Er-doped diodes, minus the Er-O implant. The bright regions show areas of high charge collection.

SEI

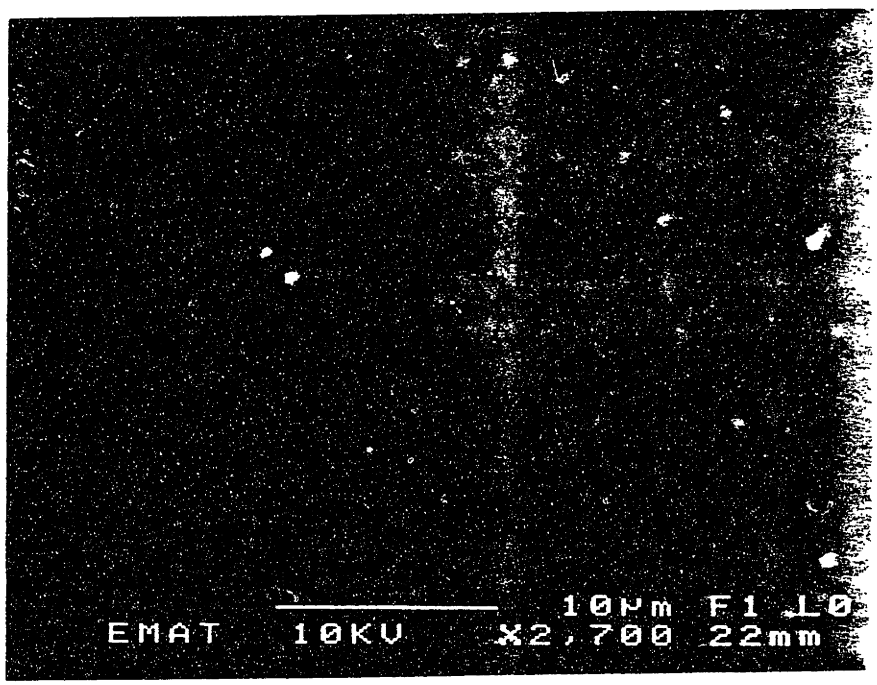

EBIC

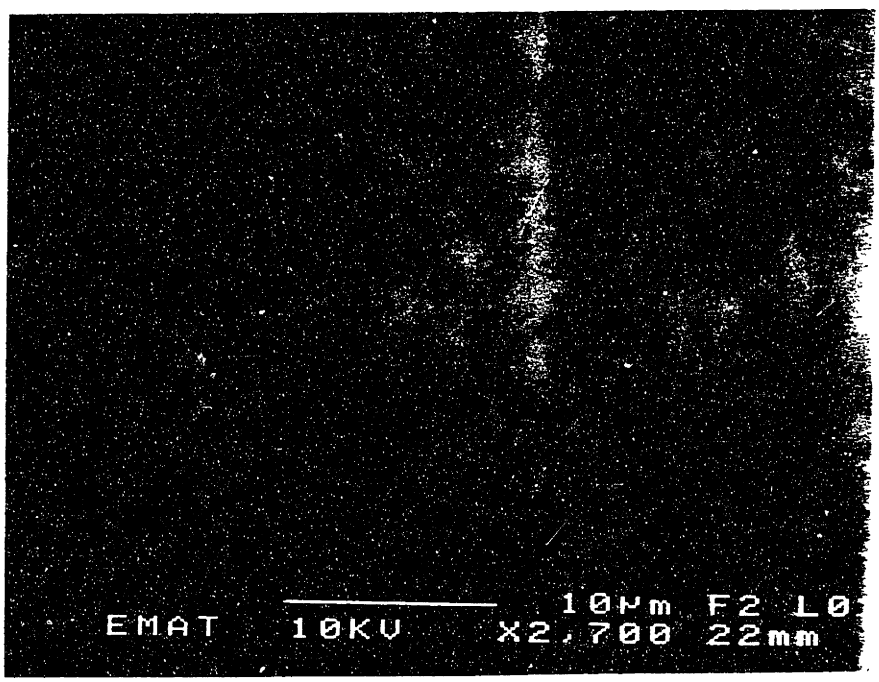

Figure 4-5: SEI and EBIC image of Si:Er LED at high magnification. 10nA. 10kV

have effects on the EBIC image, causing a disruption in the collected charge resulting from a change in the local electric potential.

The dislocations are probably not visible due to their depth and their density. Tamura has shown in studies that high energy implants result in a buried layer of defects [27]. We would expect this layer to be somewhere around 1.5 μm to coincide with the peak of the Er implant. To image something that deep, the bulk of the electron-hole pairs generated must be at that depth, requiring an accelerating voltage of about 20kV. At this accelerating voltage, the generation droplet spreads out to a fairly large sphere, of roughly 1.5 μm in diameter, resulting in poor resolution. More importantly, another problem in imaging is the proximity of the dislocations. If there are many defects and if they are close together, their images will overlap, not providing enough contrast to be imaged.

4.2.2 Quantitative EBIC measurements

The quantitative measurements from EBIC can be used to calculate charge collection efficiency of diodes, and in the case of the Si:Er LED's, can be used to determine the effects of Er in the mesa on the collected current. Efficiency measurements were taken by connecting the pin connector inside the SEM through the outside port to an ammeter, from which the collected current can be directly read. The efficiency is defined as the ratio of the collected current to the maximum expected current, I_g, given in equation 3.8. Varying the acceleration voltage gives a depth profile of the generated carriers, by varying the range of the electrons and the depth of the generation volume, as discussed in section 3.1. The signal collected can be normalized to take into account the beam current as well as the beam acceleration, using equation 3.7 for charge collection efficiency. The results are shown in Figure 4-6, which include both a reference diode without any Er, processed the same way as the Er doped diode. The high beam currents used were on the order of 1.5 nA and the low beam currents were on the order of 0.05 nA.

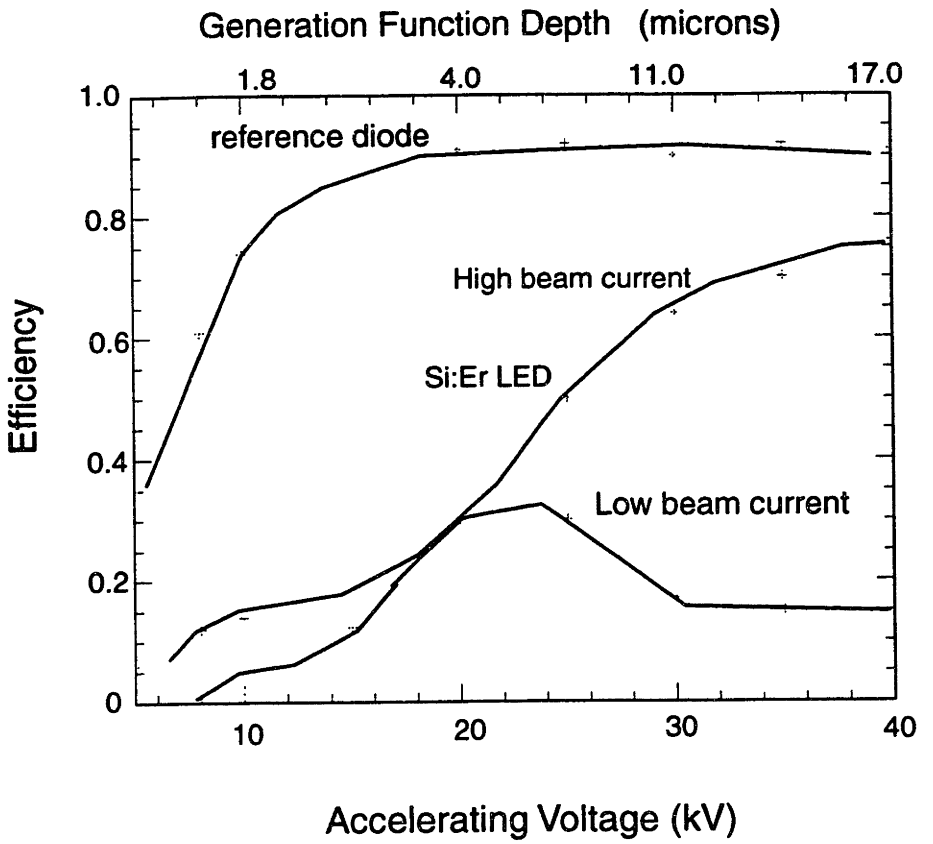

Figure 4-6: EBIC charge collection efficiency of reference diode, with no Er and O implant, and Si:Er LED at high beam currents and low beam currents.

4.2.3 Reference Diode

The reference diode is more efficient than the Er-doped diode, showing a saturation value of nearly 90% efficiency. The steep increase in efficiency occurs after the p-n junction is passed by the generation volume of the beam, at which point carriers are easily swept across the depletion width. The diffusion length is constant after the junction is passed, and is fairly long, on the order of tens of microns, shown by the carriers created deep in the sample being 90% collected at the surface.

4.2.4 Er-Doped LED under low injection

At low beam currents, all of the Er is not saturated and only a fraction of the Er is in an excited state, causing a decrease in the collected charge as the electrons recombine at the Er instead of diffusing to the surface to be collected. Because exctied Er has a long lifetime, on the order of 1 ms, saturation should be avoided in order to

use EBIC as an Er monitor. The decrease in the EBIC efficiency after the peak of the generation volume has passed the peak of the Er implant, at 20 kV, is an indication that Er acts as a very strong recombination center. Most of the carriers being generated at high beam voltages are recombining before they reach the surface, because they must diffuse through the Er implant. The low EBIC efficiency at beam voltages less than 20 kV show the presence of defects, possibly dislocations, in the material that act as recombination centers.

4.2.5 Er-Doped LED under high injection

At high beam currents, the amount of Er in the excited state is saturated, and any more carriers injected into the sample will not excite more Er ions. Because the Er layer will not capture more carriers, the excess carriers travel through the Er layer and diffuse to the surface, shown by the saturation of the EBIC efficiency levels at high accelerating voltages to an EBIC efficiency of nearly 80%.

Once all the active Er is saturated, there are three possible explanations in the interactions of carriers with the excited Er. First, there may be no further excitation of Er once an electron is in the $^4I_{13/2}$ state, and photons are only emitted at the wavelength of 1.54μm. If this is the case, the carriers would indeed diffuse to the surface and be collected as current. The second case is that the Er, after being excited to the $^4I_{13/2}$ level, traps another carrier and becomes excited to next level, at the $^4I_{11/2}$ state. If this occurs, a photon at 1.27eV would be emitted during recombination. If this photon is reabsorbed into the band, which is possible, since the band gap is 1.1eV, the effect would be the same as another carrier released into the material, and collected as current. However, the absorption coefficient is α=10cm^{-1} at 1.27eV, meaning that most of the light emitted at that wavelength will not be absorbed back into the silicon, but will escape from the surface since it is being generated at a depth of only 1.5μm [25]. If the carriers were exciting the Er to levels higher than the first excited state, the efficiency measured at the surface would peak and then start to decrease as carriers were trapped and recombined at higher energies. The third possibility is a direct excitation of the Er ions by the electrons, resulting in second,

third and possibly fourth level excitations. The probability of this occuring, is the probability of a direct collision between an Er ion and an electron which is very small, and is readily discounted. We can conclude that the Er will not capture more carriers once the first excitation level is reached, and that once an Er ion is excited into the $I_{13/2}$ level, the f-shell will not be excited to higher energy levels by recombination.

Once saturation is reached by the injected carriers, Er ceases to be an efficient recombination center. The diffusion length of the carriers after saturation is achieved is quite high, as shown by the high EBIC efficiency levels at high beam currents. A conclusion to the EBIC efficiency measurements from the arguments above show that the Er, once excited to the $^4I_{13/2}$ state, will not be further excited to higher energy states. This is an important conclusion, in that other excited states will not emit light at 1.54μm.

4.2.6 Determination of Saturation Levels

From the efficiency curves, an estimation of the saturation level can be made. From Figure 4-6, the efficiency at 20 kV is seen to be 30%, at both high and low beam current graphs. At 20 kV, EBIC current and efficiency measurements were made at various different beam currents, from 0.001 nA to 1.0nA. The lowest beam current at which a 30% efficiency measurement was found to be 0.098 nA, shown in Figure 4-7. This is assumed to be the threshold excitation level needed for saturation at 20 kV. To estimate the number of carriers that are generated at this level, the lifetime of the electrons in the silicon must be calculated. In EBIC efficiency measurements when the curve reaches a peak and then falls, the diffusion length can be estimated as the range of the electron from the SEM beam. For low beam currents, the efficiency measurement reaches a peak at about 20 kV. At this voltage, the beam range is about 4μm. If a diffusion length of 5μm is used as an estimate, the lifetime can be calculated as:

$$\tau = L^2/D_n \tag{4.3}$$

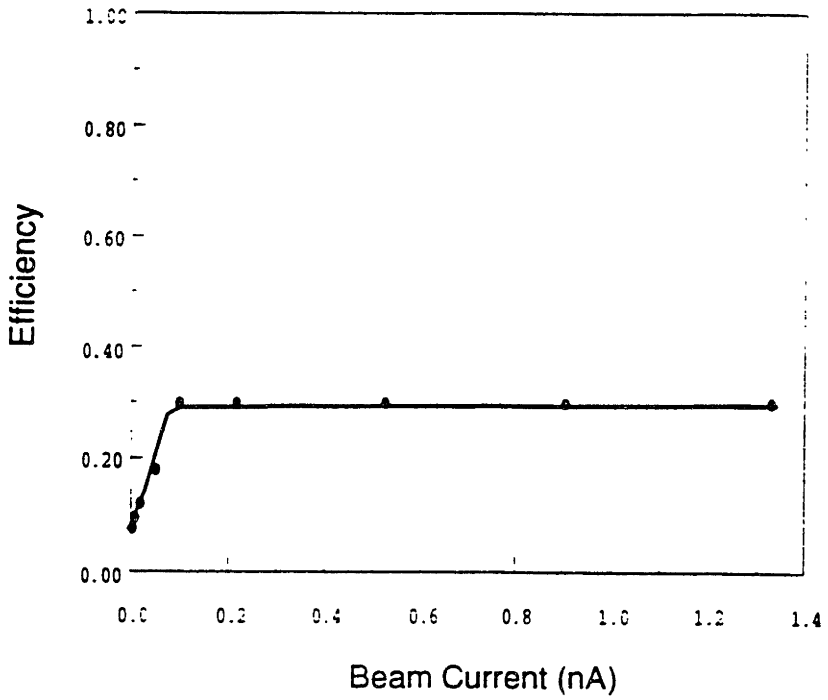

Figure 4-7: EBIC charge collection efficiency vs beam current at 20kV. The value of 30% is reached at 0.098 nA

where L is the diffusion length and D_n is the diffusion constant of electrons in Si. D_n is given as

$$D_n = (kT/q)\mu \tag{4.4}$$

D_n is calculated as $26cm^2/sec^2$, using an estimated mobility of $1000cm^2V/sec$. Using these values, τ= $1.0x10^{-8}sec$. At 0.098 nA, there are $2.56x10^{12}$ primary electrons/sec, designated by N_g, calculated using the function I_g, given in equation 3.4, divided by the charge of an electron, shown below:

$$N_g = I_g/q \tag{4.5}$$

This value of N_g calculted above is the number of carriers per second produced at the onset of saturation. Multiplying by the lifetime and dividing by the volume of the generation droplet, which was estimated to be a sphere of radius 2μm, the steady state carrier density is $1.0x10^{15}$ electrons/cm^3. This will be defined as the injectio

level of carriers needed for saturation, beyond which excess carriers produced will not excite more Er, and is given by the equation:

$$N_{primary\ electrons}(\#/cm^3) = N_g\tau/Volume \tag{4.6}$$

Calculating the injection carrier density at 30kV, for both high and low beam currents, can give an understanding of the difference in the two measurements, and the saturation levels. At low beam current, at 30 kV, the EBIC measurement was taken at 0.0130 nA. At that injection current, the carriers created are $5.07x10^{11}$primary electrons/sec. Using the same lifetime as above and a generation volume calculated from a sphere of radius 5.5μm (from the range of an electron at 30 kV), the carrier density is found to be $9.8x10^{12}$primary electrons/cm^3, using equation 4.6. At the high beam current in the measurement, which was 1.317 nA, the diffusion length cannot be estimated as 5μm any longer. Because the carriers created at high accelerating voltages are efficiently collected at the surface, the diffusion length, and thus the lifetime of the carriers in the Si, is much longer. For ideal current collection, that is 100% efficiency, the lifetime is estimated at $10^{-6}sec.$ In the LED, the efficiency is 80% because of recombination at the dislocations. Making an estimate that the lifetime is 80% of the ideal lifetime, τ can be calculated to be $8x10^{-7}sec.$ Using this lifetime and the volume of the generation drop at 30 kV in equations 4.5 and 4.6, the density of carriers is calculated to be $7.08x10^{16}$primary electrons/cm^3.

The density of carriers created by the low beam current is lower than the number needed for saturation, and the density of carriers created by the high beam current is higher than the number needed for saturation. The density of carriers created can explain the difference in the EBIC effieciency collections between high and low beam currents. At the high beam currents, since the Er is already excited, there are carriers created that will not recombine at the Er. These carriers are the ones being collected at the junction as EBIC current. The carriers created at low beam currents all recombine at the Er layer and consequently, the percentage of carriers collected at the surface are very low.

The injectio level of saturation of $10^{15}cm^{-3}$ Er, agrees very well with the levels of compensation from the C-V curve discussed in section 4.1, in which the level of electrically active Er was near $1x10^{15}cm^{-3}$. It is not known if the electrically active donors are actually the recombination centers that saturate in the EBIC measurements, but the correlation between the measurements may be significant.

4.2.7 Capture Cross Section of Er in Si

From the estimated value of the lifetime of an electron in Si at low injection currents, a rough calculation of the capture cross section, σ_n, of Er can be made. For deep centers in the gap, the capture cross section can be found as:

$$\tau^{-1} = \sigma_n v_{th} N_{Er} \tag{4.7}$$

v_{th} is the thermal velocity and is approximately $1x10^7$ cm/sec, and N_{Er} is the concentration of excited Er, which can be taken to be approximately $1x10^{15}cm^{-3}$. τ, from above, is on the order of $1x10^{-8}$ sec. σ_n is found to be $1x10^{-14}cm^2$. The value for τ is only an average value calculated from the EBIC measurements. It is probably higher than the actual value, because of the carriers created by the electron beam at 20 kV, half are created before the Er implant. These carriers diffuse to the junction much more easily than carriers created beyond the implant, and were not considered to do so in the simplified calculation of diffusion length in the section above. If τ is actually lower than the value used in this calculation, the capture cross section is a lower limit, showing that Er is indeed an effective recombination center.

4.3 Temperature Dependence of Er Signal

The temperature dependence of the Er cathodoluminescence is shown in Figure 4-8. The temperature dependence is the same that is found in the data from both PL and EL measurements citedebs. This implies that the Er is behaving the same in both a local area, in which carriers are generated from the beam in a small droplet,

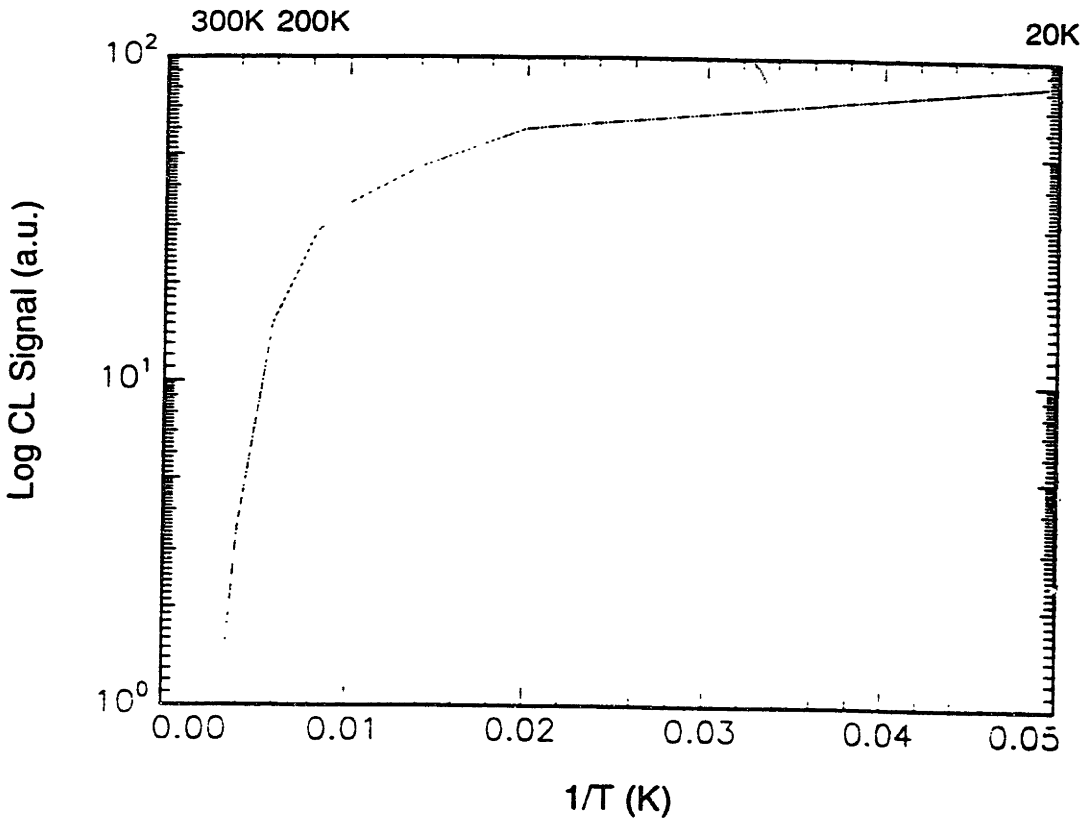

Figure 4-8: Temperature dependence of Er cathodoluminescence signal in Si:Er LED.

and in a large-scale area, in which carriers are being generated across the surface of the whole diode. It has been proposed by Ren that the thermal quenching of the Er luminescence, which is independent of processing conditions, dopant impurity, and implantation dose, is probably a consequence of energy backtransfer from the excited Er to the charge carrier system in Si[6]. He models backtransfer as a thermally activated process, dominant at temperatures greater than 200K [6]

4.4 CL Results

4.4.1 Spectra of Si:Er LED's

The Oxford cold stage was used in all CL measurements, and the detector used was a liquid nitrogen cooled Ge detector for measuring infrared light. Samples were mounted on the cold stage sample holder which was evacuated to at least a base pressure of $2x10^{-6}$ atmosphere to eliminate problems of ice formation on the sample.

The optimal signal and collection conditions for CL in our SEM were accelerating voltage of 30kV and the maximum current achievable at that voltage, which was on the order of 1.0μA. The monochrometer slit size could be varied, between 0 and 10 mm, but for good resolution with a high signal intensity, we found that slit sizes of 3-6 mm were best, giving spectral resolution of 11.7 nm to 23.4 nm at FWHM respectively. Under these conditions, all D-lines could be seen as well as the free exciton line at 1.13 μm. Typical spectra are shown in Figure 4-9 a) showing the free exciton line and D4, and b) showing D2, D3 and the Er excitation line. All lines are not visible on the same graph because the free exciton signal is very strong and it cannot be scaled under the same conditions as the lower intensity lines. A spectrum of the reference diode was also taken, and found to have only the exciton signal. The exciton signal can be used as a measure of the quality of the silicon. The stronger the signal, the better the material, because there are fewer electron-hole recombination centers. Under normalized conditions, that is, conditions in which the beam current and accelerating voltage are factored in using equation 3.9, the exciton line of the reference diode was higher than the LED, shown in Figure 4-13. This is another indication that the LED has more recombination centers, which are the dislocations and Er luminescence lines that appear in the spectra.

4.4.2 Comparison of Fabricated Structures

Five different samples were compared in CL for their spectra, which are as follows:

1. Er/O implanted sample with junction and mesa (A typical Si:Er LED)
2. Er/O implanted sample with junction, but without mesa
3. Er/O implanted sample without junction and without mesa
4. Sample with just junction and mesa (A reference diode)
5. Sample with just junction, without mesa

All samples were prepared in the Microtechnology lab at MIT, using standard processing procedures, and the samples without mesas were processed using the same

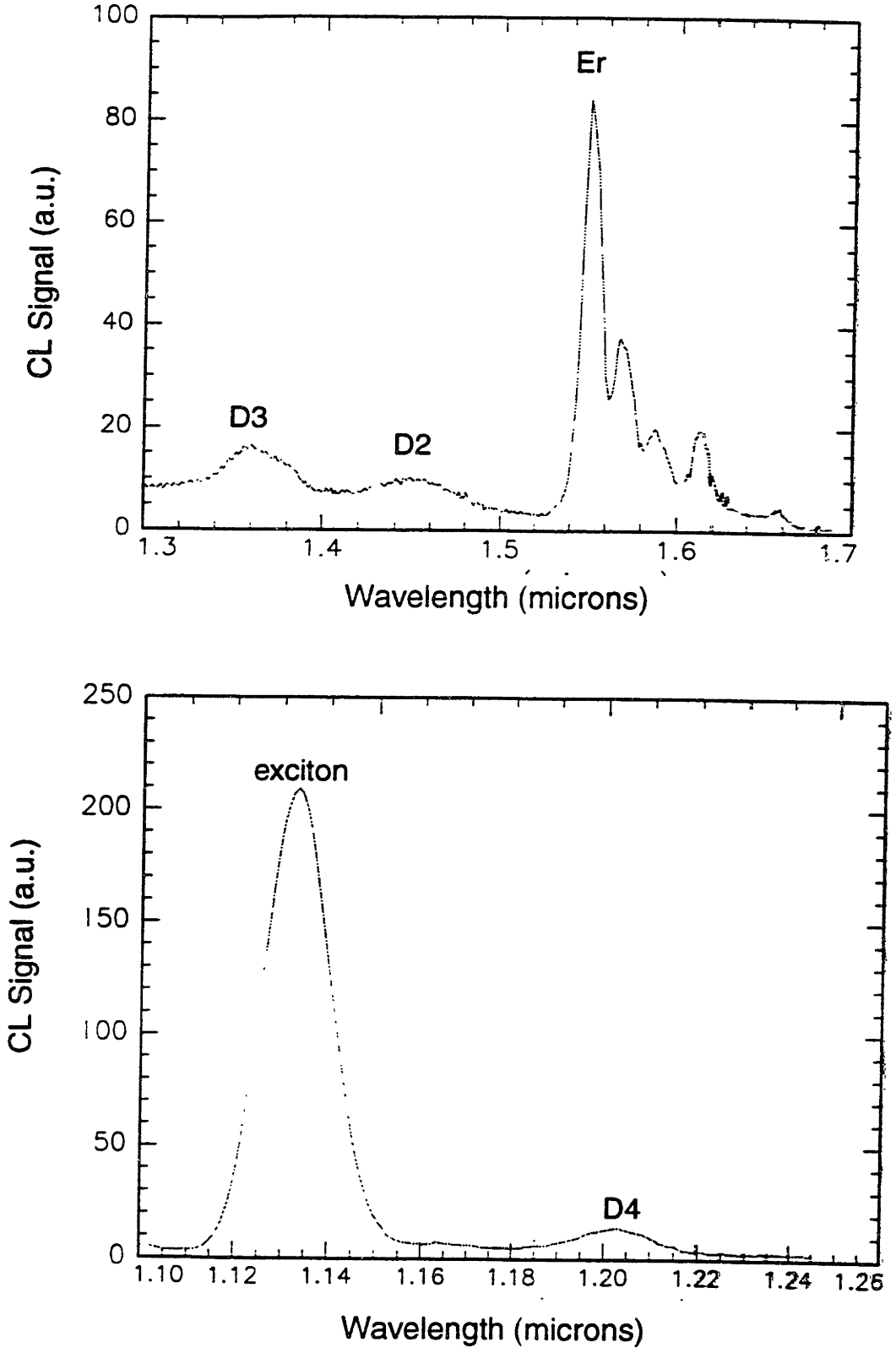

Figure 4-9: Si:Er LED spectra taken at 20K.a)showing Er, D3 and D2. b)showing exciton and D4

processing steps and equipment as the mesa diodes, minus the patterning and etching of the mesas, LTO deposition, and Al contact and patterning.

Since the LED and the reference diode had undergone the same processing steps, except of course, the Er and O implant, the lack of D-lines in the reference diode sample show that the formation of the mesa, especially the RIE etch, which is a destructive technique, is not the cause of the dislocations. The high dose implant of the junction by itself is not the cause of the dislocations, even though the junction implant caused amorphization. The damage induced by the junction implant was successfully annealed out.

The D-lines were seen in the samples with only the Er/O implants (no mesas), both with and without the junction implant, which implies that the damage induced during the high energy Er and O implants caused dislocations to form during annealing. To test this hypothesis, CL spectra of Er/O implanted samples were taken after annealing in an argon atmosphere. The spectra showed no sign of D-lines, shown in Figure 4-10, which makes the processing of our LED's in a nitrogen and oxygen ambient the prime suspect in the formation of dislocations. To determine if the problem is indeed the ambient or if it is the annealing process in MIT's Microtechnology Lab, causing the dislocations, an Er/O implanted sample was annealed in a clean furnace in both nitrogen and argon atmospheres, for 30 minutes at 900°C. In both cases, the samples did not exhibit dislocation related spectra. It can be concluded that the furnace annealing in the MTL is the responsible step in the formation of dislocations.

4.4.3 Depth Profiles

By varying the accelerating voltage and collecting spectra, a depth profile of the signal can be obtained, as explained in chapter 3. The normalized signals are shown in Figure 4-11, of the Er signal, D2 signal and D3 signal. The peak of the generation function is included in the graphs. The Er signal reaches a peak at about 20kV at 20K. At this accelerating voltage, the peak of the generation volume is 1.3μm, near the Er implant peak. The peak luminescence is consistent with the EBIC efficiency measurements, in that the collected charge increases at 20kV, where the peak of the

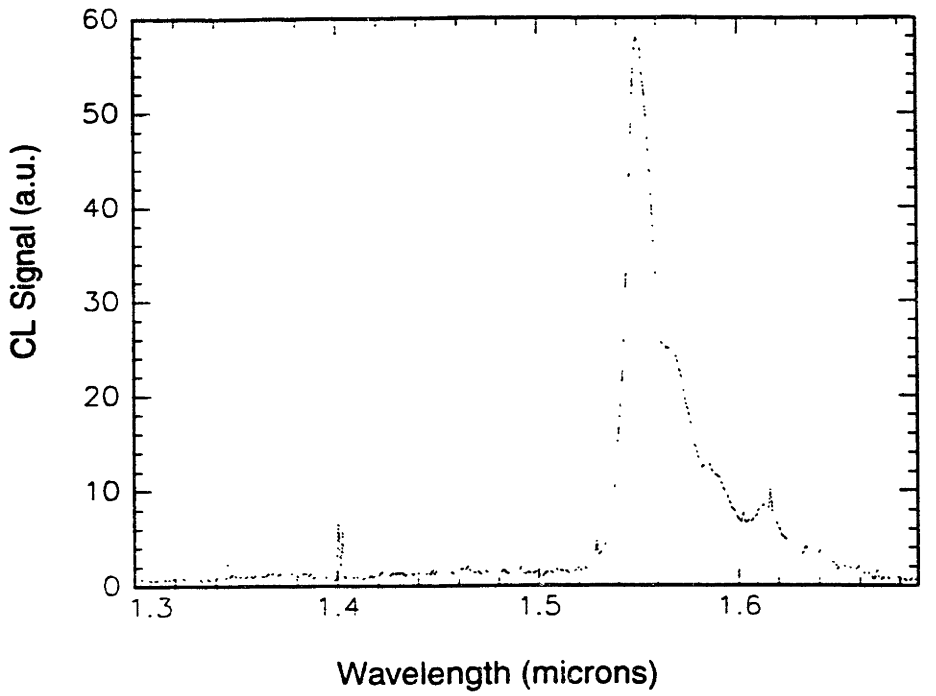

Figure 4-10: CL spectra of Er/O implanted Si annealed at 900C, 30 min in argon.

generation function reaches the depth of the Er implant. The spectra for D2 and D3 do not reach a peak, but level off. This can be explained in two ways. First, the dislocation may be very deep, beyond the depth that can be reached with the highest accelerating voltage of 40kV. This would make the depth of the dislocations close to 5 μm, the peak of the generation volume at 40kV. The second explanation is that the Er and D-line luminescence are competing processes, and the D-line signal actually reaches a peak at nearly the same place as the Er peak, but since the Er is a more efficient recombination center, the D-line peak is suppressed. This would put the dislocations at a depth of about 2 μm, which is a more reasonable approximation. The dislocations are in a layer from the surface through the implanted region of the Er, and is consistent with the effects of high energy implantation, causing damage near the implant, as discussed in chapter 2.

To understand the shape of the depth profile, the Er luminescence signal can be modeled using the Er implant distribution and the carrier generation function g(z), eq. 3.4, where $z = x/R_e$, where R_e is the range of the electron at a given accelerating

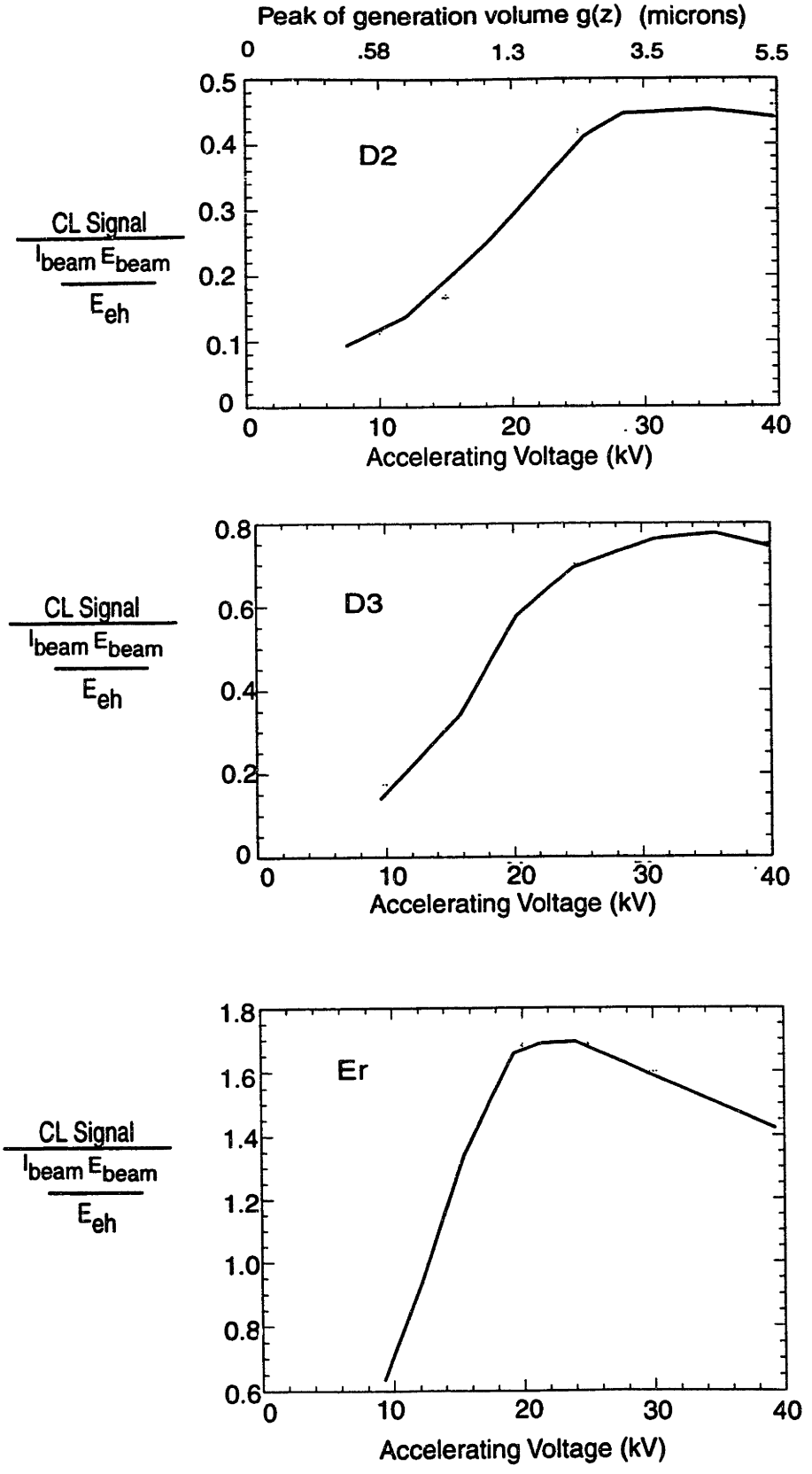

Figure 4-11: CL Signal vs Accelerating Voltage of the Er, D2, and D3 signals, 20K.

voltage. The gaussian distribution of the Er implant is modeled using TRIM, and was found to have a straggle of 0.5μm, at a range of 1.5μm. A first approximation of the signal can be made using the following integration:

$$Er\ signal = \int g(z)[Er] \tag{4.8}$$

The signal was calculated for accelerating voltages from 10 kV to 40 kV, resulting in the graph shown in Figure 4-12, which also shows a normalized signal intensity of the Er luminescence. The signal calculation is only a first approximation because it does not take into account the diffusion of carriers in the substrate, but it corresponds with the measured signal profile, by exhibiting a peak at an accelerating voltage of 20 kV. The calculated values at higher accelerating voltages are lower than the measured signal because of the diffusion of carriers back towards the Er layer. From the calculated values, we can be sure that the depth profiles of the luminescence signals are being interpreted correctly, and that the Er implant maintains a gaussian profile with its peak at 1.5μm, after device processing.

The free exciton line was also compared at different acceleration voltages, shown in Figure 4-13 of both the reference sample and the LED. The LED exciton line is in each case lower than the reference LED, showing that the LED does indeed have other recombination centers that are taking away from the exciton line. The LED's exciton signal was added to the Er and D-line signals to compare with the reference LED, shown in Figure 4-14. By adding all the signals to the exciton line, all the radiative recombination processes seen in our spectrum are taken into account. The fact that the added signal does not equal the reference diode signal is an indication that there are probably nonradiative recombination processes occurring in the LED or radiative processes beyond the range of our detector and monochrometer system. The nonradiative recombination processes may take the form of multiphonon interactions, energy backtransfer loss from the Er, or Auger processes.

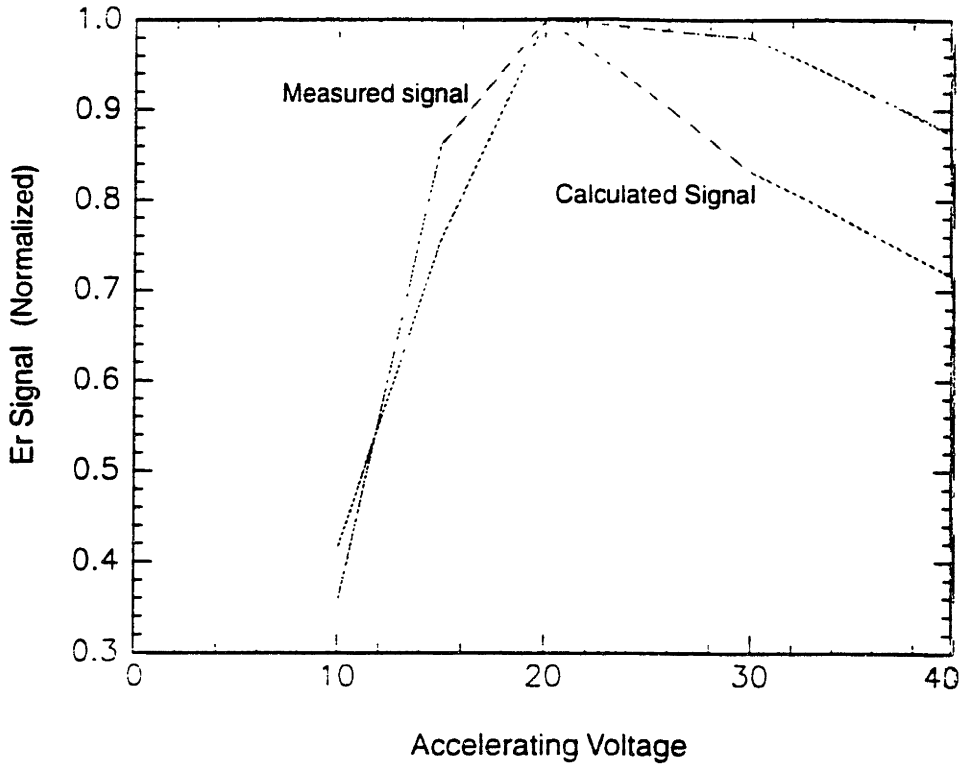

Figure 4-12: Calculated Er signal vs. acceleration voltage.

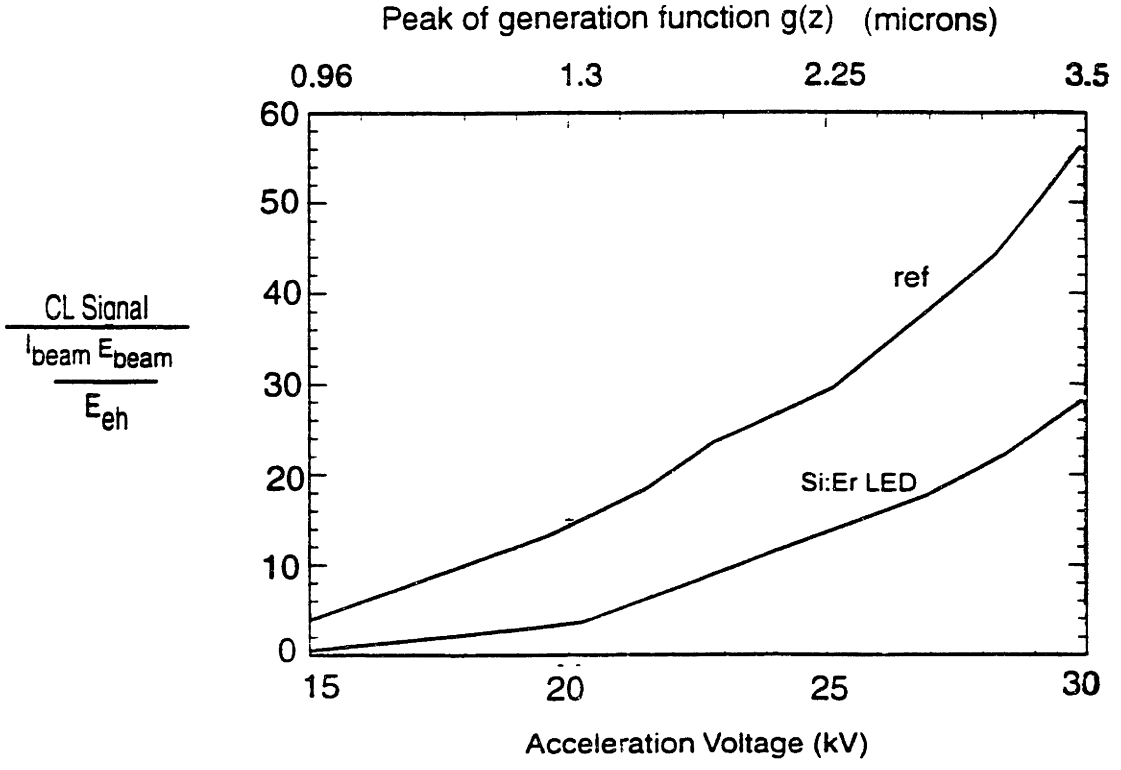

Figure 4-13: CL Signal vs acceleration voltage of exciton line, 20K

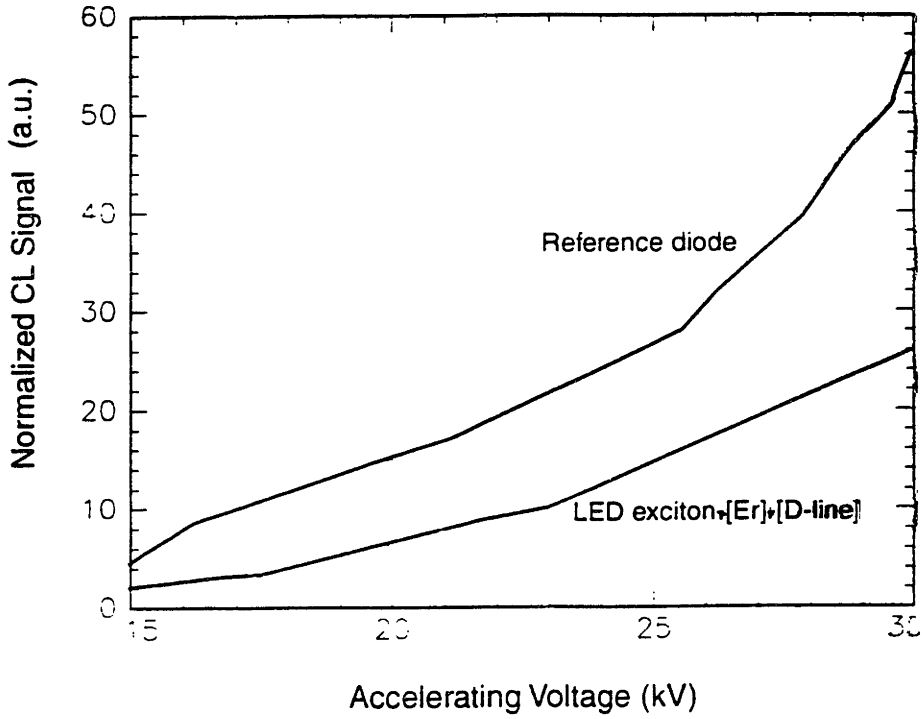

Figure 4-14: LED exciton+[Er]+Dline signals and reference diode signal.

4.4.4 Processing Problems with Mesa Etch

Er was found in the CL spectra on the substrate of the diodes in set PB-4, but not in C-2. Although the signal was small, it was definitely an indication of Er on the substrate between the etched mesas, and corresponds with the electrical connection of diodes across the substrate in EBIC images. There could be two reasons for this. The first being that the mesas were not etched to the proper depth of 3 μm, and the second being that the Er implant had a straggle that reached a depth of below 3μm. From SIMS data of Er implanted into Si at 1.5μm at 4.5 MeV, and annealed, it can be seen that the Er gaussian profile peaks at 1.5μm, and extends out to 3 μm, shown in Figure 4-15. An etch depth of 3μm is sufficient to remove the Er from the substrate between the mesa structures, and form electrically isolated devices. It is very possible that CL is sensitive to lower concentrations than the SIMS measurement, and even at concentrations lower than 10^{15} cm^{-3} Er, luminescence of Er is seen. The ratio of the substrate Er signal to the mesa Er signal is approximately 1:40. If the substrate

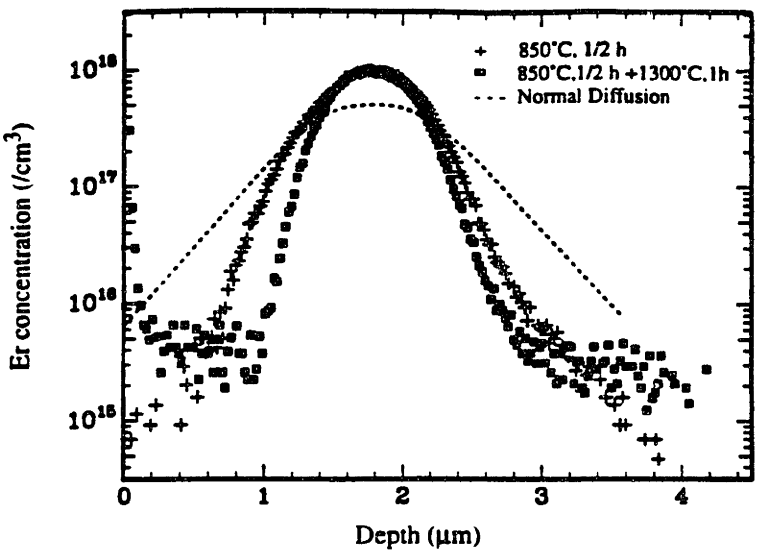

Figure 4-15: SIMS profile of Er implanted in Si with a peak depth of 1.5μm after a 850°C anneal at 30 min [6].

concentration is $1x10^{15}cm^{-3}$, the signal on the substrate as compared with the mesa is expected to be approximately 100 times lower, with the assumption that the signal is linear with the concentration of Er ions. The ratio is within experimental error of the expected value.

To investigate the second reason for Er on the substrate, the mesa step height of the diode in question was measured using Dek-Tak step height measurements, and found to be 2.7μm. Other diodes that did not exhibit Er on the substrate had step heights of over 3μm. In the case of this diode set, the insufficient etching is the cause of the electrical connection and traces of Er on the substrate. The RIE etch step is very important and proper care must be taken to ensure that the mesa step height is high enough. Of samples measured, the step heights varied from 2.7 μm to 3.8μm. The discrepancy is a signal that the RIE etch step is nonuniform between runs and is unreliable in depth.

4.5 Defect Imaging

The spectrometer used in the CL setup and a PGT computer used for electron dispersive X-ray spectroscopy (EDX) were modified in an attempt at mapping the D-lines with CL. The mapping was set at a speed of 0.15 second per point, at 256 points on the screen, under which conditions the mapping would take approximately 30 minutes for an area of about $1.25mm^2$. In the efforts to map the dislocations, the brightness levels consistently increased over the time of the mapping, causing the images to be all bright with no areas of contrast. This is probably due to sample charging, from the oxide on the surface, in which case there is no solution to the problem. The D-lines may also be too deep to image, due to a loss of resolution, in the same manner that EBIC could not image the defects. It is possible for dislocations and other defects to be seen during a spectroscopic scan and not during imaging [31].

Another method used to image the defects was etching using a preferential Secco etch, resulting in etch pits at the defects. First the diodes were stripped of their aluminum in a solution of 1:2 HCL:H_2O, and then the oxide was removed in 1:1 HF:H_2O and finally the diodes were Secco etched in 2:1 HF:$K_2Cr_2O_7$. The diode was examined in the SEM and etch pits were seen all over the surface of the mesa, shown in Figure 4-16, along with the area surrounding the mesa is shown after etching. The difference in the topography between the two samples is the RIE etch on the areas surrounding the mesa, resulting in a rougher surface.

The difference in the two areas shown in the figures is apparent. The dislocation density is estimated to be about $10^8 cm^{-3}$ based on the etch pit count, which is a very high number of dislocations. A reference diode was etched for comparison and is shown in Figure 4-17, in which very few pits are seen. To correlate the etch pits to the D-line spectra, the etched sample was put in the cold stage for low temperature CL measurements and a pit was focused on. The SEM beam was placed in spot mode, in which the beam does not raster across the whole screen, but stays on a spot designated by cross hairs on the CRT. A spectra was taken at the pit, and then the cross hairs were moved to a spot beside the pit and another spectra was taken with

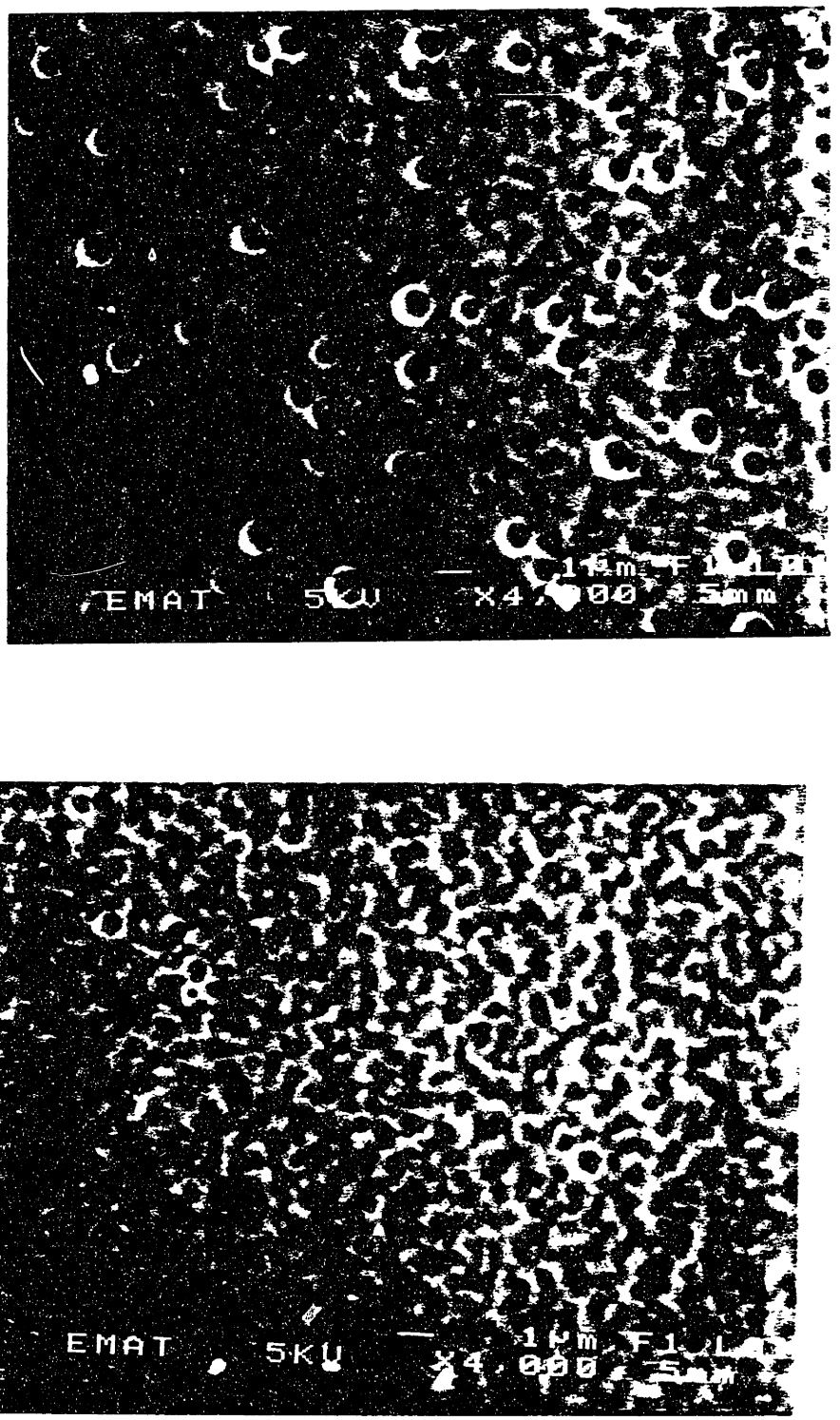

Figure 4-16: a) Etch pits on the surface of the mesa of LED, and b)etched areas surrounding the mesa.

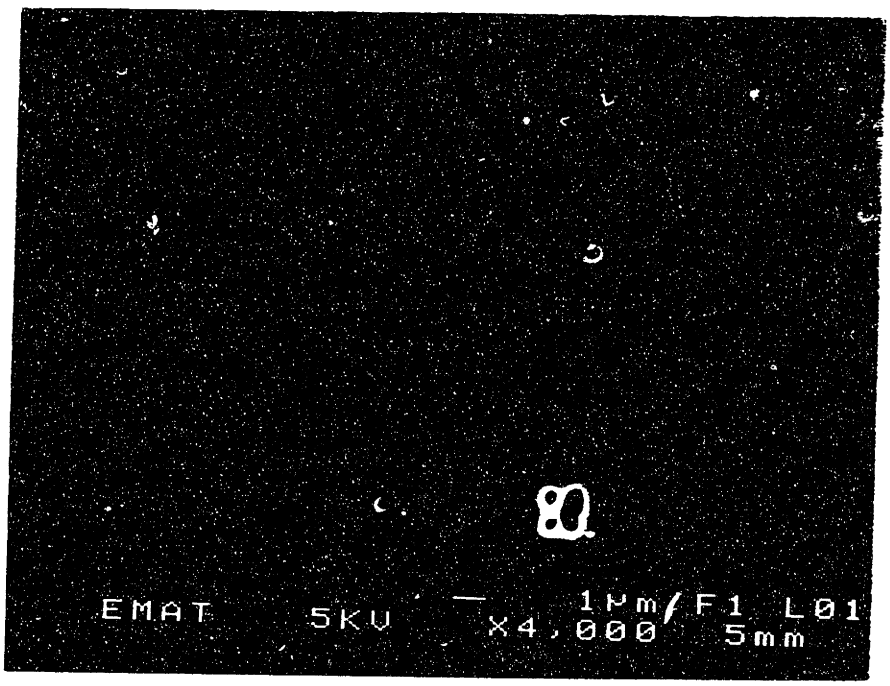

Figure 4-17: An etched reference diode, showing few dislocation pits.

exactly the same collection conditions. The Er signal in the two spectra were the same, but the D-line spectra at the etch pit was higher than the signal surrounding the etch pit. The ratios are given in Table 4.1.

There were problems associated with the CL spectra of the etch pits. The current that is needed in the cold stage to image well is very high, on the order of 0.5μA, because of the metallic shielding around the sample for thermal insulation. The SEI detector is behind the metallic shielding, so much of the signal from the sample is scattered away. Due to high currents and high voltages needed to image well, the resolution was very poor. As a result, all of the etch pits seen under normal imaging conditions could not be seen. Only the very dark, deep pits were seen, and it is possible that the spectra was taken on another, shallower etch pit where there was thought to be none. Another problem in the spectra of dislocations is that there is a high chance that they are curved, that is they are not coming straight out of the substrate. If this is the case, it is difficult to ensure that the electron beam is hitting them correctly, which would affect the signal, both in the areas at the dislocations, making their signal lower, and beside the dislocation, making their signals higher. The Er signal may have remained constant for both measurements because the resolution is so low. With the generation volume peak at 30 kV at 3.5μm, the Er being excited is not just coming from the area of the beam spot, an argument that can be used for the dislocation signals as well. Under the difficult circumstances this was probably the best measurement method possible.

In ideal circumstance, the signal at the etch pit should be high and the signal beside it should be close to zero. Under the circumstances used in this measurement, including poor resolution, diffusion of carriers, and curved dislocations, the fact that there is a difference in the signals at all is encouraging. In examining the mesa, the number of pits seen on the surface is very large, but there seemed to be a pattern, in that there were even more pits near the center of the LED.

To understand the distribution of the D-lines, point scans, in SEM spot mode, were done across an LED. The result was a spectroscopic map of the D-lines, showing a maximum of both D-line signals (D2 and D3) near the center of the mesa. The

Table 4.1: Comparison of CL signals in etch pit to other regions on the mesa.

Wavelength	Signal at Pit	Signal Beside Pit	Ratio
1.36	33	24	1.375
1.45	20	14	1.43
1.54	43	42	1.02

results are plotted, normalizing the signals and then adding the signals together to obtain an arbitrary total signal unit. The results are mapped in Figure 4-18, in which a) is a schematic of the LED and b) is the defect signal mapped across the diode, showing the peak at the center. The same result was found when mapping the diode in a direction perpendicular to that shown. The data corresponds with the conclusion, made from the CL depth profiles, that the dislocations are deep and originate at the implant. The dislocations in the center are farthest away from any surface, and consequently they are the most difficult to anneal out.

4.6 Saturation of Er Signal

From EL, PL, and EBIC studies, it has been seen that the Er signal saturates at high injection levels, as shown in Figure 4-19 showing the EL spectra with a variation in drive current density. An equivalent measurement using CL is to take measurements at a given accelerating voltage and vary the beam current, increasing it to get saturation. The results are shown in Figure 4-20, taken at 20K, at which temperature about 10% of the Er is optically active. The CL luminescence increases steeply and is probably a sign that saturation is reached almost immediately, but is not seen as

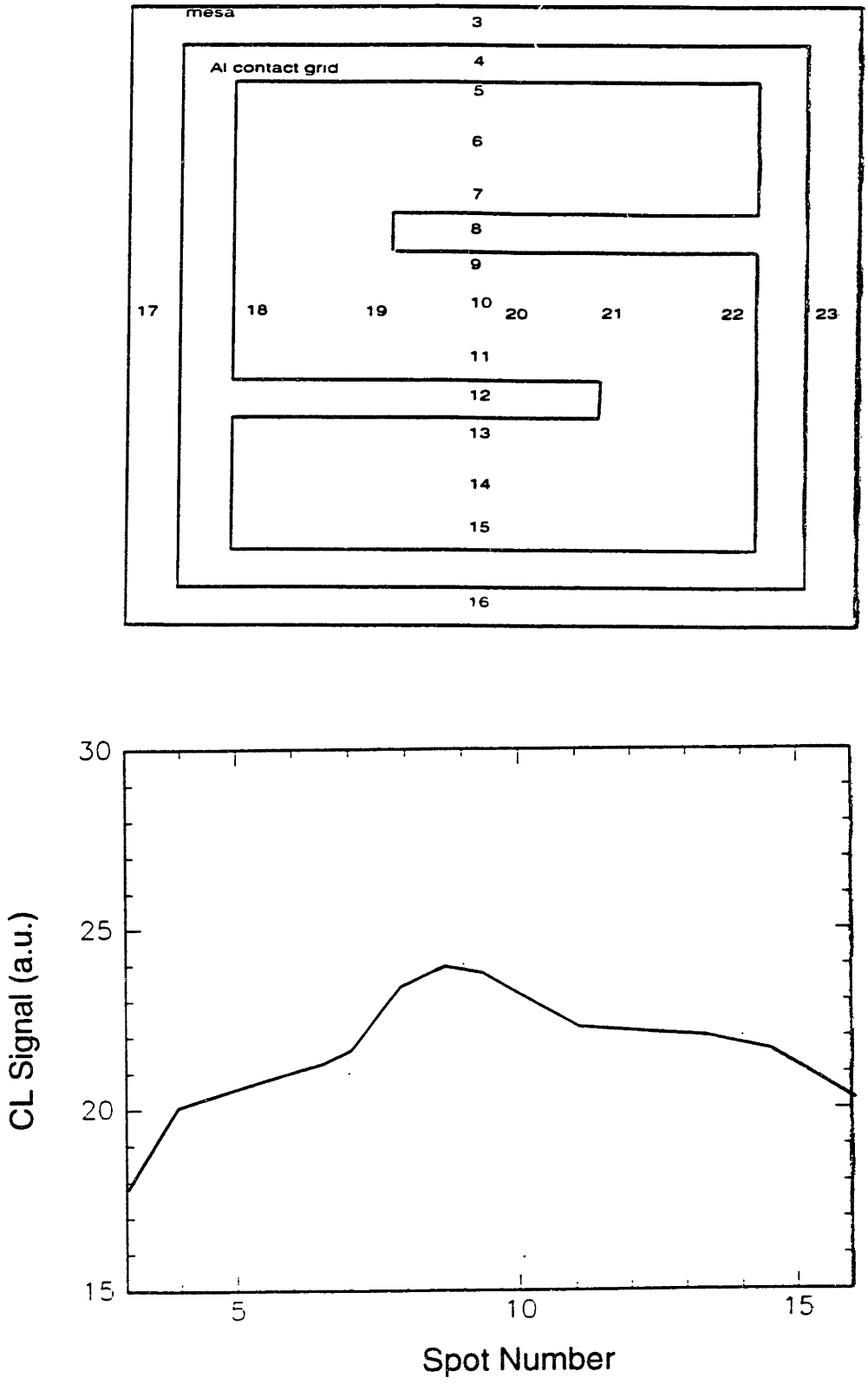

Figure 4-18: Defect map. a) A schematic of the LED measured. and b)the defect signal in the added units.

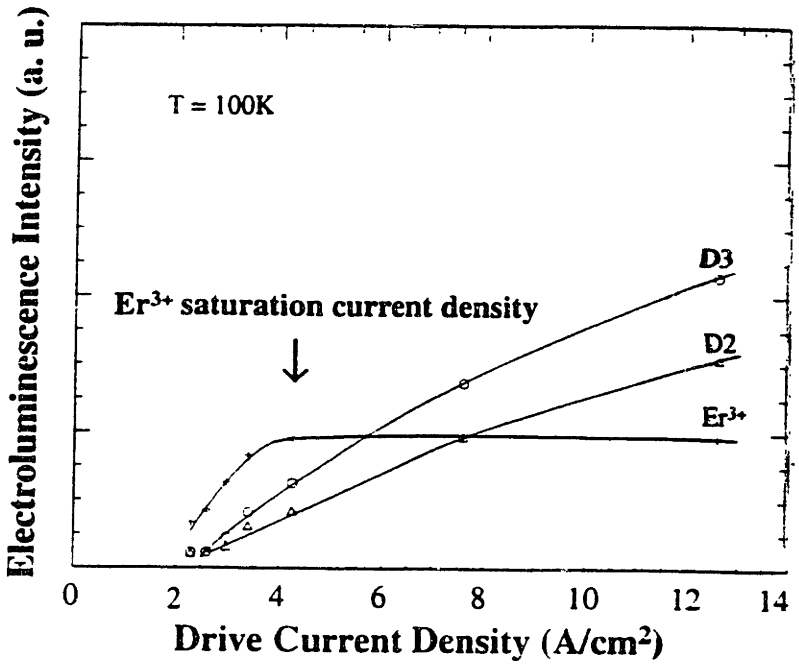

Figure 4-19: EL intensity of signals with varying drive current density at 100K

such in the graph because the detecton system used is not sensitive enough when a small area is luminescing. The CL and EL differ slightly because the two methods have different ways of exciting and collecting the luminescence. In CL, the carriers are excited in a small area and are generated deep in the sample, whereas in EL and PL the carriers are generated on the whole surface of the sample being studied

The Er saturates at high injection levels because of its long lifetime in the excited state of about 1 ms. All the active Er becomes excited, and the ions in the excited state are waiting to decay and emit photons at low temperatures, therefore, higher injection currents will not cause any extra emission intensity [6]. This is corroborated by the EBIC efficiency measurements taken at high and low injection currents, where at high injection currents, the Er is saturated and any excess carriers will not recombine at the Er and excite more Er. The luminescence intensity is in essence limited by the long lifetime of the Er, but may not be at its maximum, due to the dislocation recombination sites that are seen in the spectra. In the sample annealed in an argon atmosphere, the peak Er signal from CL is approximately 3 times higher

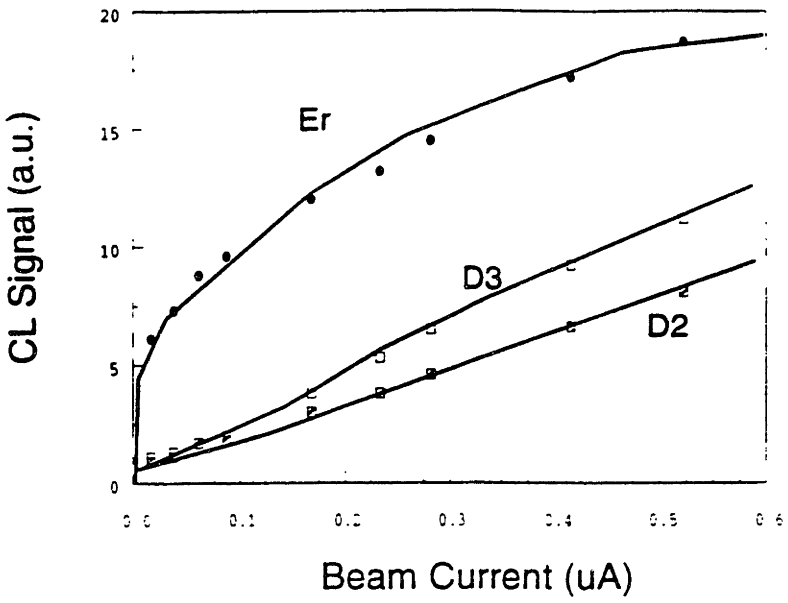

Figure 4-20: CL intensity of signals at 30kV, with varying beam current at 20K.

than the signal of the Er structures that have D-lines in their spectra, under identical measurement conditions. The Er signal is higher without dislocations in the silicon, which is as to be expected, showing that more carriers are recombining at the Er and not at the dislocations.

The saturation of the Er signal in CL can be corellated with the saturation of the excited Er in EBIC. At the high injection levels used in CL to read a luminescence signal, the excited Er will already be saturated, seen by the levels of injection needed for EBIC saturation. This is shown by the fact that D-line luminescence is seen at the lowest signals at which Er luminescence is seen. The fact that the injection currents must be so high to see any luminescence is a limit of our detection system, which may not be sensitive to very low levels of light generated in small areas. The light that is seen is due to the diffusion of carriers to much larger areas than the generation droplet created by the beam, because the current is so high.

From the measurements described in this chapter, there are different processes of recombination occurring when carriers are injected into Si:Er LED's. These include

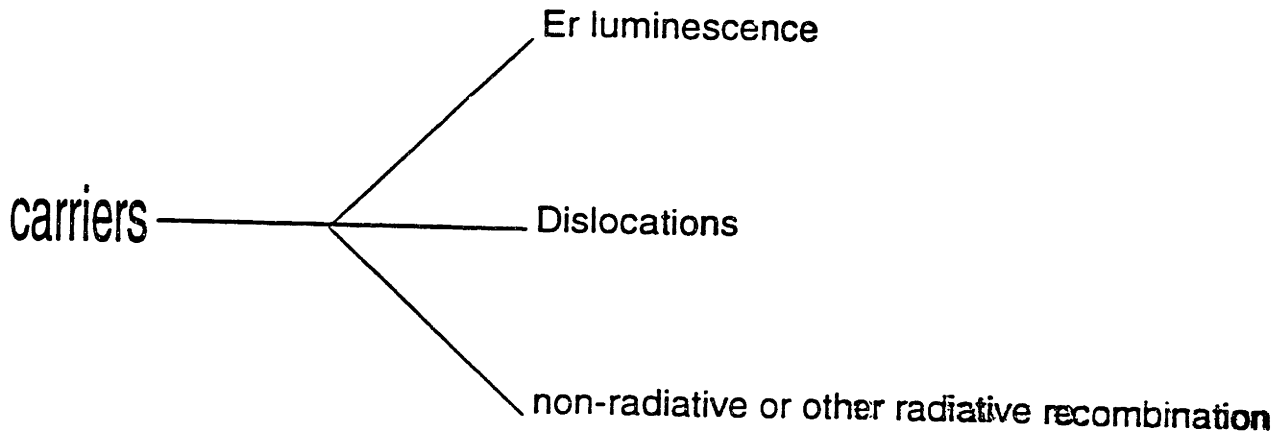

Figure 4-21: A schematic of the different recombination methods in Si:Er LED's.

are Er excitation, recombination at dislocations, and non-radiative recombination or radiative recombination at wavelengths beyond the scope of the detector. These processes are shown schematically in Figure 4-21

Chapter 5

Conclusions and Future Work

To use Er doped Si to its full potential as an optoelectronic material, the luminescence from the Er de-excitation must be maximized. Only when strong room temperature luminescence is realized will Si:Er become a viable material in the microelectronic industry to initiate Si based optoelectronic technology. The dislocations must be eliminated and other processing parameters must be optimized before the LED's are high quality devices with strong room temperature luminescence.

5.1 Donor Characteristic of Er in Si

From the C-V measurements of Si:Er LED's, we can be sure that the Er is exhibiting donor characteristics. The Er compensates the background doping, which is shown in the measurement as a dip in the free carrier concentration. The interaction of the donor characteristics of Er with the optical characteristics should be understood well to ensure that luminescence is optimized. The background dopant levels of the wafer can then be altered to provide the best environment for Er luminescence. Studies involving different background dopant concentrations and different donor levels of Er should be very useful in achieving maximum light output with given Er concentrations. The shape of the C-V curve also indicates that the electrical measurement is consistent with the SIMS profile of the Er implantation being a gaussian profile, even after the many processing steps involved in making a device.

The electrically active Er is seen to compensate the p-region to about $1x10^{15}cm^{-3}$, which is in agreement with the levels of carriers that need to be generated by the electron beam in EBIC in order to saturate the active Er. The role of the donor activity of Er with recombination is not completely understood, but the results found here may be the first step in understanding the relationship.

5.2 Causes and Effects of Dislocations

In chapter 4, different fabricated structures were compared for their Er and D-line luminescence intensity. The mesa structures as well as the wafers with Er and O implanted in them all showed signs of D-lines in their spectra. After the Er/O implant, the processing steps for the diodes are few. They include annealing in nitrogen, low temperature oxide deposition, and Al contact masking, deposition, patterning and sintering. The aluminum contact steps were not included in the Er/O wafers that were included in the CL studies, so those steps are not responsible for the dislocations. The LTO deposition step was not part of the wafer processing either, leaving only the anneal as the step responsible for dislocation formation. The sample annealed in argon did not exhibit D-line luminescence, making the annealing step the primary suspect in the production of the dislocations. From the studies of samples annealed in a nitrogen atmosphere in a clean furnace, we can be certain that the nitrogen gas is not causing the dislocations. One possibility in causing the dislocations is impurities in the furnaces. If the impurities are fast diffusing interstial-substitutional elements, like Cu or Fe, a $900°C$ anneal would cause enough diffusion into the substrate to interact with any residual damage from ion implantation. The diffusion coefficient, D_o for Cu is $4.0x10^{-2}cm^2/s$ and the activation energy, E_o is 1.0 eV. If the diffusion coefficient is calculated at $900°C$, D= $4.0x10^{-2}cm^2/s$, for Ni, D= $1.3x10^{-2}cm^2/s$, and for Fe, D= $6.2x10^{-3}cm^2/s$. Once the metals diffuse into the damaged regions of the Si as point defects, they can interact with the damaged regions and prevent proper annealing to occur, causing dislocations to form. Another school of thought on transition metals is that they are needed in defective areas to actually cause the

dislocations to luminesce [19]. If this is the case, which is in itself a much argued and discussed point, a question would arise as to whether the samples annealed in a clean furnace have dislocations that are simply not luminescing. Further studies must be done on the interaction of our LED's with transition metals.

Other variables are the ramping time of the anneal, the time it takes to load the sample into the furnace, and the quenching time after annealing. Rapid thermal quenching as opposed to slow cooling may cause different point defect agglomerations, and may in turn cause different defect states to form in either case. Since the anneal is the critical step in the cause of the dislocations, it must be monitored well in the future.

From the interpretation of the CL data, the Er implant is indeed a gaussian profile, and its luminescence can be modeled using the gaussian distribution of the implant and the generation volume of carriers created by the electron beam in the SEM. If it is assumed that the Er is a very efficient recombination center and the luminescence of the Er and dislocations is a competetive process, the dislocations are also seen to be at the depth of the implant, discussed in chapter 4. EBIC efficiency measurements show a highly defective region from acceleration voltages before about 20 kV, seen by the low collection efficiency. This is consistent with the CL measurements in estimating the depth of the dislocations. Deep dislocations are difficult to anneal out of the diode, because they are far away from the surface, which act as dislocation sinks during annealing.

From the etch pit counts, we can estimate the dislocation density of about 10^8 cm^{-2}. Such high dislocation densities, are an indication of bad device quality and inefficient recombination of carriers when compared to the reference diodes. The high dislocation density is also a reason for the inability to image dislocations, either by CL or EBIC. With such high densities, the contrast of the dislocations from either measurement method will overlap, resulting in insufficient contrast to image.

Because the CL signal of Er implanted material without dislocations is higher than the signal of the material with dislocations, the dislocations are affecting the device quality. The dislocations are competing for the carriers generated by the electron

beam in CL, causing the Er luminescence to be lower that in the case of dislocation free material. This is seen by the CL spectra of the sample without D-lines compared to the sample with D-lines. Both samples have the same concentration of Er and O implanted, but the normalized signal of the sample without dislocations is three times higher than in the sample with dislocations under identical measurement conditions. As the carriers are generated, and diffuse toward the depletion region in the junction, some recombine at dislocations. If nonradiative recombination processes are ignored, seemingly only 1/3 of the electron hole pairs recombine at the Er. However, there are either nonradiative recombination centers in the devices or luminescence centers that were not scanned by our spectrometer, which can be seen by comparing the exciton lines in Figure 4-13. From the experimental results, the dislocations are affecting the performance of the diodes, and should be eliminated to result in higher Er luminescence, and better device performance.

5.3 Saturation of Er in Si

Saturation of excited Er is an important reason for a limit to the Er luminescence intensity at room temperature. From EBIC efficiency measurements, at high injection currents, the active Er saturates, and the excess carriers diffuse to the surface without exciting any more Er. At low injection levels, the Er is not completely saturated, and all the carriers generated are used to excite the Er, showing that Er is a very efficient recombination center. The Er luminescence intensity levels off with higher injection levels, and more current will not provide stronger luminescence. A very rough estimate of the capture cross section of Er^{+3} was calculated, and found to be on the order of $10^{-14}cm^2$.

An important conclusion of the saturation of the collected current in the EBIC efficiency measurements is the fact that excess carriers will not cause more excitation in the Er 4f-electron shell. Extra carriers will not cause a higher excitation level after the 4f level has been excited to the $^4I_{13/2}$ state. An important consequence of this conclusion is that the excited Er will only emit light at 1.54μm, so extra injection

will not cause a decrease in the Er luminescence signal.

From the EL saturation curves in Figure 4-19, the Er signal saturates at high injection levels, while the D-line signals continue to increase. This can be explained with the previous argument. As the optically active Er saturates, extra carriers can only recombine at the dislocations, causing a higher dislocation luminescence spectrum. At low injection currents, the dislocations do not luminesce strongly because the Er is a more efficient recombination center and the carriers recombine there before the dislocations. This conclusion is consistent with the previous section, in which it was stated that the dislocations take away from the Er luminescence. The dislocations still luminesce at low injection before saturation of the Er takes place, and will always cause some percentage of carriers from the total injection level to recombine. A 900°C anneal has been shown to maximize the Er-O complex formation, and minimize defect formation and in turn, maximize the Er luminescence signal [6]. If defect formation is not being minimized, we cannot be sure that the luminescence is at its maximum level.

Thermal saturation of Er occurs at room temperature and the Er signal drops to almost negligible levels, most likely due to electron energy backtransfer, a thermally assisted process. The nonradiative energy released from the Er de-excitation is transferred to the Si lattice through phonon interaction. If backtransfer is occuring and because it is a thermally activated process, it is very dominant at room temperature, and will cause the luminescence signal from the Er to be lower. This is seen in Figure 4-8, in which the luminescence signal of Er falls off rapidly above about 200K. The fact that the luminescence behaves the same way in EL and CL shows that Er behaves the same under local injection currents, by the electron beam in CL, and a "global" injection current, across the whole diode in EL.

5.4 Processing Optimization

To fabricate high quality Si:Er LED's, a few processing steps must be changed. The problem of mesa structures being underetched can be eliminated by using the pro-

cessing steps used in diode set C-2. In this set, the mesas were etched first and the Er was implanted through a mask, with openings in the areas to be implanted. The photoresist mask was 3μm thick which, through simulations, is seen to be thick enough to stop the Er before it reaches the substrate. This avoids any Er, no matter how little the concentration, from staying on the substrate areas between the mesas, ensuring electrical isolation.

Another processing parameter to be changed is the co-dopant ligand that is used to enhance Er luminescence. The ligand F gives the highest Er luminescence in Si. Using F may cause the Er luminescence to be higher at room temperature, if the dislocations are eliminated. Further studies including different ligands with Er should be done in the future, to optimize the light output.

Of most importance to creating high quality devices is the processing step responsible for the dislocation production. Through systematic elimination, it has been determined that the annealing step to remove the implantation damage is the step responsible for dislocation formation. The annealing of the LED's must be monitored very carefully, in order to eliminate dislocations in the substrate. The variables to be tested are the impurity concentrations in the annealing furnaces, the temperature ramps, the time it takes to load the sample into the furnace, and the cooling process.

5.5 Other Future Work

Once the processing parameters of the Si:Er LED's are optimized, dislocations in the devices should be eliminated. Since it is estimated that less than 1% of the Er is optically active at room temperature, higher concentrations of Er should be incorporated into the Si lattice. Low temperature CVD is an ideal method by which to increase the Er concentration, which will surpass the concentrations achievable by ion implantation. Another benefit of CVD will be an elimination of a damaged layer from implantation to anneal. Without the implantation damage, there will be no dislocations. A study which may be of considerable importance is the electrical characterization of Er in wafers with different background doping levels. The lumi-

nescence may increase as the electrical activity is changed. A relationship between the electrical activity and the optical activity should be studied to understand the interaction between the donor characteristics and the luminescence intensity.

Although it has been established that Er is a donor in the Si lattice thorough C-V measurements, its states in the gap are virtually unknown. DLTS measurements of the Si:Er LED's will provide valuable information about the trap levels of Er when fabricating devices. In addition to the trap levels, the capture cross sections of Er^{3+} should be determined by DLTS and compared with the results found here, as a measure of how effective Er is as a recombination center.

EBIC efficiency measurements at low temperature should be performed, to estimate the difference in saturation levels at low temperature and room temperature. If the saturation currents are higher at low temperature, this may give a clue as to the optically active levels of Er at room temperature, and how much of an increase in luminescence higher concentrations of Er in Si will provide. The backtransfer phenomenon should be studied as well, in order to better understand the processes ocurring to cause a nonradiative recombination to occur.

Once defect free diodes can be fabricated in the facilities at MIT, there will be better chances of room temperature luminescence. As of yet, an actual physical limit to the luminescence of Er in Si has not been found. Future work in this area will ensure that process and device optimization is achieved, and problems including defects will be overcome, as well as weak luminescence at room temperature. As work continues in this field, an opto-electronic system will be fabricated, including strong emittors, waveguides, amplifiers, and modulators, and Si:Er will become a viable tool in the optoelectronic industry.

Bibliography

[1] H.S. Hinton. *IEEE Spectrum*, page 42, Feb 1992.

[2] O. Wada, T. Kamijoh, and M. Nakamura. *Circuits and Devices*, page 37, Nov. 1992.

[3] J.D. Crow. *IEEE*, page 20, March 1991.

[4] J. LaCourse. *IEEE*, page 27, March 1992.

[5] H. Ennen, J. Schneider, G Pomerenke, and A. Axmann. *Appl. Phys. Lett.*, 43(10):943, Nov 15 1983.

[6] F.Y.G. Ren. *Silicon Doped Erbium as an Optoelectronic Semiconductor Material.* PhD thesis, Massachusetts Institute of Technology, May 1994.

[7] D.J. Eaglesham, J. Michel, E.A. Fitzgerald, D.C.Jacobson, J.M. Poate, J.L. Benton, A. Polman, Y-H. Xie, and L.C. Kimerling. *Appl. Phys. Lett.*, 58(24), 17 Sept 1991.

[8] J. Michel, J. L. Benton, R.F. Ferrante D.C. Jacobson, D.J. Eaglesham, E.A. Fitzgerald, Y-H. Xie, J.M. Poate, and L.C. Kimerling. *J. Appl. Phys.*, 70(5):2772, Sept. 1 1991.

[9] L.C. Kimerling, D.M. Koker, B. Zheng, F.Y.G. Ren, and J. Michel. *Semiconductor Silicon*, chapter Erbium Doped Silicon for Integrated Optical Interconnects. Electrochemical Society, Princeton, N.J., 1994.

[10] R. Sauer, J. Weber, and J. Stolz. *Appl. Phys. A*, 36:1–13, 1985.

[11] Y.S Tang, K.C. Heasman, W.P. Gillin, and B.J. Sealy. *Appl. Phys. Lett.*, 55(5):432, July 31 1989.

[12] P.B. Klein and G.S. Pomrenke. *Electron. Lett.*, 24:1503, 1988.

[13] B.E.A. Salek and M.C. Teich. *Fundamentals of Photonics.* John Wiley and Sons, New York, NY, 1991.

[14] J. Michel, F.Y.G. Ren, B. Zheng, D.C. Jacobson andJ.M. Poate, and L.C. Kimerling. The physics and applications of si:er for leds. *Proceedings of ICDS 17*, 1994.

[15] J.L. Benton, J. Michel, L.C. Kimerling, D.C. Jacobson, Y-H Xie, D. J. Eaglesham, E.A. Fitzgerald, and J.M. Poate. *J. Appl. Phys.* 70(5):2667, Sept 1 1991.

[16] J.L. Benton, D.J. Eaglesham, M. Almonte, P.H. Citrin, M.A. Marcus, D.L. Adler, D.C. Jacobson, and J.M. Poate. *Mat. Res. Soc. Symp. Proc.*, 301:119, 1993.

[17] W. Wijaranakula. *J. Appl. Physics*, 70(6):3018, Sept 1991.

[18] J. Palm. Private communication.

[19] V.Higgs, E.C. Lightowlers, C.E. Norman, and P. Kightley. *Mat. Sci. Forum*, 83-87:1309, 1992.

[20] N. A. Drozdov, A.A. Patin, and V.T. Tkachev. *Phys. Stat. Solidi A*, 64:K63, 1981.

[21] K. Werbnek, J. Weber, A. Hopner, F. Ernst, R. Buchner, M Stefaniak, and H. Alexander. *Mat. Sci. Forum*, 83-87:1315, 1992.

[22] J.S. Williams and J. M. Poate, editors. *Ion Implanting and Beam Processing.* Academic Press Inc., New York, NY, 1984.

[23] S.K. Gandhi. *VLSI Fabrication Principles for Si and GaAs*, page 4. John-Wiley and Sons, New York, NY, 1983.

[24] J. F. Ziegler, editor. *Handbook of Ion Implantation Technology.* North-Holland, New York, NY, 1992.

[25] S. M. Sze. *VLSI Technology*, pages 355–359. McGraw Hill, New York, NY, 1988.

[26] H. Sayama, A. Kimomura, Y. Yuba, and M. Takai. *Nucl. Inst. and Meth. B*, B80/81:587, 1993.

[27] M. Tamura. *Materials Science Reports*, 6:141–214, 1991.

[28] A. Polman, J.S. Custer, E. Snoeks, and G.N. van den Hoven. *Nucl. Inst. and Meth. B*, B80/81:653, 1993.

[29] S.M. Davidson and C.A. Demitriadis. *J. Microscopy*, 118:275.

[30] H.J. Leamy. *J. Appl. Phys.*, 53(4):R1, June 1982.

[31] B.G. Yacobi and D.B. Holt. *J. Appl. Phys*, 59(4):R1, Feb 15 1992.

[32] C.A. Klein. *J. Appl. Phys.*, 39(4):2029, March 1968.

[33] T.E. Everhart and P.H. Hoff. *J. Appl. Phys.*, 42(13):5837, Dec 1971.

[34] J.I. Hanoka and R.O. Bell. *Ann. Rev. Mater. Sci.*, 11:353–380, 1981.